Bulletin of the Seismological Society of America

Impact of Site-Response Characterization on Probabilistic Seismic Hazard in the Po Plain (Italy)

--Manuscript Draft--

Manuscript Number:	BSSA-D-22-00177R3
Article Type:	Article
Section/Category:	Regular Issue
Full Title:	Impact of Site-Response Characterization on Probabilistic Seismic Hazard in the Po Plain (Italy)
Corresponding Author:	Simone Barani University of Genoa Genoa, ITALY
Corresponding Author's Institution:	University of Genoa
Corresponding Author E-Mail:	simone.barani@unige.it
Order of Authors:	Claudia Mascandola
	Simone Barani
	Dario Albarello
Abstract:	We present a probabilistic seismic hazard analysis for the entire Po Plain sedimentary basin (Italy), one of the widest Quaternary alluvial basins of Europe, to evaluate the impact of site-response characterization on hazard estimates. A large-scale application of the Approach 3 of the U.S. Nuclear Regulatory Commission (NRC) to include seismic amplification in the hazard is presented. Both 1D amplification related to stratigraphic conditions and 3D amplification due to basin effects are considered with the associated uncertainties, and their impact on the hazard is analyzed through a sensitivity analysis. While 3D basin effects are considered through the application of an empirical, spatial invariant correction term, 1D amplification was estimated throughout the study area by means of dynamic (equivalent-linear) ground-response analysis. To separate aleatory variabilities and epistemic uncertainties related to site response, a partially non-ergodic approach is used. The results provide a finer picture of the actual seismic hazard, highlighting those areas where the ground motion is affected by amplification effects due to local or regional geological features. We found that, for a return period of 475 years, neglecting basin effects produces a 30% underestimation of the seismic hazard in the long-period (> 1s) range. Moreover, with reference to the hazard model adopted, such effects are responsible for most of the epistemic uncertainty (up to 80%) in the results. Therefore, such effects deserve special attention in future research related to probabilistic seismic hazard analysis in the Po Plain sedimentary basin.
Author Comments:	Dear Editor, given the recent call for papers on a special BSSA issue on Seismic Hazard Modeling, we were wondering if our manuscript could be published therein. I look forward to hearing from you kind regards SB
Suggested Reviewers:	Chris Cramer Research Professor, The University of Memphis ccramer@memphis.edu Expertise in Probabilistic Seismic Hazard and Risk Analysis, Uncertainty in Hazard and Loss Estimates.
	Paolo Bazzurro

	Professor, IUSS Pavia paolo.bazzurro@iusspavia.it Expert in hazard and risk assessment for earthquakes and other natural events. We applied his method in our study.
	Marco Pagani Seismic Hazard coordinator, GEM Fundation marco.pagani@globalquakemodel.org He has strong professional skills in Probabilistic Seismic Hazard Analysis. He is the lead developer of the scientific component of the OpenQuake-engine hazard analysis software.
	Aybige AKINCI Researcher, INGV aybige.akinci@ingv.it Senior researcher with long experience in seismic hazard analysis.
Opposed Reviewers:	
Response to Reviewers:	
Additional Information:	
Question	**Response**
Key Point #1: <i>Three key points will be printed at the front of your manuscript so readers can get a quick overview. Please provide three COMPLETE sentences addressing the following: 1) state the problem you are addressing in a FULL sentence; 2) state your main conclusion(s) in a FULL sentence; and 3) state the broader implications of your findings in a FULL sentence. Each point must be 110 characters or less (including spaces).	We evaluate the impact of 1D and 3D site-response characterization on seismic hazard in the Po Plain
Key Point #2:	3D amplification produces a 30% increase in the hazard and contributes the most to its epistemic uncertainty
Key Point #3:	To reduce the epistemic uncertainty in the hazard, the characterization of basin effects needs to be improved

Impact of Site-Response Characterization on Probabilistic Seismic Hazard in the Po Plain (Italy)

Mascandola C.[1], Barani S.[2*], and Albarello D.[3,4]

[1] Istituto Nazionale di Geofisica e Vulcanologia (INGV), Milano (Italy)

[2] Dipartimento di Scienze della Terra, dell'Ambiente e della Vita (DISTAV), Università degli Studi di Genova, Genova, Italy

[3] Dipartimento di Scienze Fisiche, della Terra e dell'Ambiente (DSFTA), Università degli Studi di Siena, Siena, Italy

[4] Consiglio Nazionale delle Ricerche, Istituto di Geologia Ambientale e Geoingegneria, Rome, Italy

[*]Corresponding author

Simone Barani

Address: Corso Europa 26, 16132, Genova

Phone: +39 010 353 8097

email: simone.barani@unige.it

Abstract

We present a probabilistic seismic hazard analysis for the entire Po Plain sedimentary basin (Italy), one of the widest Quaternary alluvial basins of Europe, to evaluate the impact of site-response characterization on hazard estimates. A large-scale application of the Approach 3 of the U.S. Nuclear Regulatory Commission (NRC) to include seismic amplification in the hazard is presented. Both 1D amplification related to stratigraphic conditions and 3D amplification due to basin effects are considered with the associated uncertainties, and their impact on the hazard is analyzed through a sensitivity analysis. While 3D basin effects are considered through the application of an empirical, spatial invariant correction term, 1D amplification was estimated throughout the study area by means of dynamic (equivalent-linear) ground-response analysis. To separate aleatory variabilities and epistemic uncertainties related to site response, a partially non-ergodic approach is used.

The results provide a finer picture of the actual seismic hazard, highlighting those areas where the ground motion is affected by amplification effects due to local or regional geological features. We found that, for a return period of 475 years, neglecting basin effects produces a 30% underestimation of the seismic hazard in the long-period (> 1s) range. Moreover, with reference to the hazard model adopted, such effects are responsible for most of the epistemic uncertainty (up to 80%) in the results. Therefore, such effects deserve special attention in future research related to probabilistic seismic hazard analysis in the Po Plain sedimentary basin.

Key Points

- We evaluate the impact of 1D and 3D site-response characterization on seismic hazard in the Po Plain.
- 3D amplification produces a 30% increase in the hazard and contributes the most to its epistemic uncertainty.
- To reduce the epistemic uncertainty in the hazard, the characterization of basin effects needs to be improved.

Introduction

It is well known that the severity and frequency content of the ground shaking at a site are significantly affected by local stratigraphic and geomorphological features (e.g., Stone et al., 1987; Seed et al., 1990; Cramer 2006; Ameri et al., 2009; Bradley 2012; Massa et al., 2014; Mascandola et al., 2017; Felicetta et al., 2021). It follows that a probabilistic seismic hazard analysis (PSHA) based on the assumptions of level ground and exposed bedrock defines only a rough, basic representation of the expected ground motion in a certain period of time, which need to be refined through detailed site-response characterization. In-depth hazard assessments that account for local amplification effects are mandatory for the design of critical facilities (e.g., dams, oil and gas pipelines, nuclear power plants) and recommended to update seismic norms, which typically scale the seismic action through the application of predefined factors. The latter are defined as a function of simple proxies (e.g., time-averaged shear wave velocity in the top 30 m of the subsoil, $V_{S,30}$) that are roughly representative of the subsoil and its effect on the seismic ground shaking. Indeed, they only account for site amplification due to shallow deposits (up to a few tens of meters deep), and disregard the effect of deep seismic impedance contrasts, which are common in deep sedimentary basins. This is the case of the study area, the Po Plain (Northern Italy), which is one of the widest Quaternary alluvial basins of Europe, with an extension of about 50,000 km^2 (Figure 1a). The Quaternary deposits in this basin are rather homogeneous throughout its extension, but deep stratigraphic discontinuities exist (from hundreds of meters to a few kilometers deep), also due to the presence of the Alpine and Apenninic buried thrust belts (e.g., Martelli et al., 2017; Figure 1a). These discontinuities are responsible for significant amplifications at long periods (> 1s; e.g., Luzi et al., 2013; Abraham et al., 2015; Lanzano et al., 2016; Mascandola et al., 2021). Therefore, a PSHA that incorporates seismic amplification effects poses a significant challenge for this region, considering its high population density, strategic role on the Italian economy due to the presence of important industrial districts (e.g., related to the oil and gas production, agriculture), and in the light of the damaging 2012 seismic sequence (e.g., Burrato et al., 2012; Luzi et al., 2013; Meroni et al., 2017).

In recent years, site-specific seismic hazard assessments that account for seismic amplification in the Po Plain area were carried out by Faccioli et al. (2015) and Vanini et al (2018), but extensive large-scale studies are still lacking. In this area, detailed hazard mapping inclusive of site effects is nowadays possible thanks to the increasing number of seismic microzonation studies (e.g., Lai et al., 2020; Martelli and Ercolessi, 2020) and ground-response assessments (e.g., Mascandola et al., 2021). Examples elsewhere are those of Cramer et al. (2004, 2006, and 2014) and Barani et al. (2020).

In this study, we perform a PSHA that includes site-response characterization on a regional scale by using the so-called Approach 3 of the U.S. Nuclear Regulatory Commission (NRC) (McGuire et al. 2001), which was originally proposed by Bazzurro (1998) (see also Bazzurro and Cornell, 2004). Our study takes advantage of previous research of Mascandola et al. (2019, 2020, and 2021) for the Po Plain sedimentary basin, which aimed at mapping the seismic bedrock and investigating the role of deep soil deposits on ground-motion amplification. Particularly, Mascandola et al. (2021) defined a soil amplification model, which focuses primarily on the long-period response (i.e., 1-3 s), by means of a 1D (equivalent-linear) ground-response analysis performed for each node of a regular grid covering the plain (Figure 1a). Compared to the predictions of the ground-motion attenuation model for Northern Italy by Lanzano et al. (2016), the results obtained from the 1D numerical analyses reflect in greater detail the spatial variability of the subsoil but neglect the 3D amplification related to basin effects, with a consequent underestimation of the surface ground motion (Mascandola et al., 2021). Similar results were observed for other sedimentary basins worldwide (e.g., Smerzini et al., 2011; Moczo et al 2018; Kato et al 2021; Aristizabal et al., 2022).

In the following, we describe the methodology implemented to include both 1D and 3D soil amplifications in the PSHA. Then, we present the hazard model used in the computations and the logic tree adopted to manage the epistemic uncertainties in the model. Given the scope of the work, which focuses primarily on the incorporation and impact of amplification effects on the hazard rather than on the assessment of the best possible hazard for the study area, only the uncertainties affecting the assumptions related to ground-motion characterization are considered. Results are then presented in terms of hazard maps for different response periods and uniform hazard spectra for selected sites. These are discussed in relation to known regional geological features and compared to those obtained by assessing the hazard through the conventional $V_{S,30}$-driven ergodic approach. Finally, the sensitivity of the hazard and its uncertainty to the 1D and 3D amplification components is discussed in detail.

A Note on Geological Setting

The Po Plain sedimentary basin is located between the thrust belts of the Alps and the Apennines (Pieri and Groppi, 1981; Carminati and Doglioni, 2012) (Figure 1a). From Late Cretaceous onwards, the thrusting of these two chains loaded and flexed the continental crust, leading to the formation of foredeep basins with a thick syn-orogenic clastic sequence (Doglioni (1993) and references therein) and a complex buried tectonic structure characterized by the south-verging thrust system of the Alps and the north-verging thrust system of the Apennines (Figure 1a).

Overall, the sedimentary succession is regressive, with deltaic to continental Quaternary sediments that overlie marine sediments of the Pliocene-lower Pleistocene (Muttoni et al., 2003; Scardia et al., 2012; Martelli and Romani, 2013). Together, the continental and marine sedimentary layers form the thick Plio-Quaternary succession, which reaches a thickness of about 8 km in the Apennine foredeep (Pieri and Groppi, 1981). The Plio-Quaternary succession directly overlies the deep Miocene sedimentary rock, which corresponds to geologic bedrock. Mascandola et al. (2019) have distinguished between geologic, engineering, and seismic bedrock. The first is defined according to the geological evolutionary history of the study area, the second is based on shear-wave velocity (i.e., $V_S \geq 800$ m/s according to the European Committee for Standardization (2004) and Ministero delle Infrastrutture e dei Trasporti (2018)), and the third is defined by a marked seismic impedance contrast where the value of V_S associated with the deep layer approaches or exceeds 800 m/s. According to these definitions, geologic, engineering and seismic bedrocks may not coincide. In the following, we will consider the seismic bedrock as the reference rock site condition.

Combining geophysical and geological data, Mascandola et al. (2019) mapped the seismic bedrock depth. Subsequently, Mascandola et al. (2021) defined a seismostratigraphic model for the sedimentary cover down to the seismic bedrock (i.e., first hundreds of meters) by means of 3D interpolation of several 1D shear-wave velocity profiles obtained from microtremor array measurements and borehole tests. A NW-SE cross-section from this model, showing the variation with depth of both the seismic bedrock and the shear-wave velocity of the overlying sediments, is presented in Figure 1b. Note the deepening of the seismic bedrock towards the south-eastern sector of the Plain, which implies amplification effects at longer periods (Mascandola et al., 2021).

Methodology

In recent years, significant progress has been made in the field of site-specific PSHA. The works of Faccioli et al. (2015), Barani and Spallarossa (2017), and Aristizabal et al. (2022) provide a comprehensive review of the different approaches for the integration of seismic amplification into PSHA. The fully probabilistic approaches can be grouped into three levels of increased complexity. The simplest one is based on the use of ground-motion prediction equations (GMPEs) for generic ground types defined according to the proxies (e.g., $V_{S,30}$) adopted by building codes for the purpose of site classification. The second amends an existing GMPE with a site-specific, period-dependent (or -independent) amplification factor determined from 1D, 2D, or 3D numerical simulations, regression analysis on ground-motion data (i.e., the site term, $\delta S2S_s$, is quantified by the systematic deviation of the observed ground motion at site *s* with respect to the median predicted ground motion), or Standard Spectral Ratios (SSR). The more complex one, which was originally developed by Bazzurro (1998) and published by Bazzurro and Cornell (2004) later on, convolves the rock hazard curve for the site under study with the probability distribution of the amplification at that site. This method is also referred to as Approach 3 of the U.S. NRC (McGuire et al., 2001). This latter method has two main advantages: it breaks the problem in two parts (i.e., it separates the PSHA for rock site conditions and the ground-response assessment), thus facilitating the hazard computation, and allows for non-linear soil effects. Recently, Barani and Spallarossa (2017) upgraded the convolution method by separating the epistemic contribution associated with the uncertainty in the soil properties from the aleatory variability in site amplification due to the different input motions used in the ground-response assessment.

The approaches mentioned above can be applied either with or without the ergodic assumption. According to the conventional ergodic PSHA, the ground-motion variability from a large data set of ground motions, from various earthquakes recorded at multiple stations, is an unbiased estimate of the variability at a single site (Anderson and Brune, 1999). Hence, the total ergodic ground-motion standard deviation (commonly known as "sigma", σ) mixes known (or knowable) and random residual components:

$$\sigma = \sqrt{\tau^2 + \phi^2} = \sqrt{\tau^2 + \phi_{S2S}^2 + \phi_{SS}^2} \quad (1)$$

where τ and ϕ are the between-event and within-event standard deviations, ϕ_{S2S} quantifies the site-to-site variability, and ϕ_{SS} is the event-corrected single-station standard deviation (e.g., Al Atik et al., 2010; Rodriguez-Marek et al., 2011).

Conversely, the non-ergodic approach separates those components that are known (or knowable) because of their repeatable nature, thus allowing for a better representation of the ground-motion sigma. In the present study, we apply the so-called partially non-ergodic approach to avoid double counting of the uncertainty related to site response (e.g., Rodriguez-Marek et al., 2014; Faccioli et al. 2015; Mascandola et al., 2017; Barani et al., 2020). Compared to the fully non-ergodic approach, the partially non-ergodic one separates only the repeatable and systemic component related to the site behavior from the ergodic sigma, while ignoring those components that are related to earthquake source and wave path (Lin et al., 2011; Villani and Abrahamson, 2015). The standard deviation for the partially non-ergodic approach is known as the single-station sigma (Atkinson, 2006), and is given by:

$$\sigma_{SS} = \sqrt{\tau^2 + \phi_{SS}^2} \qquad (2)$$

In simple words, in the partially non-ergodic approach the ground-motion standard deviation is reduced by an amount (ϕ_{S2S}) that reflects the uncertainty affecting the site amplification term.

Following Rodriguez-Marek et al. (2014), three essential requirements are needed to apply a partially non-ergodic PSHA approach: (1) the median value of the site-specific amplification (or de-amplification) term must be properly estimated, and both (2) the epistemic uncertainty in site amplification and (3) the epistemic uncertainty in the single-station standard deviation must be taken into account. In order to determine the site amplification term, which expresses the average deviation of ground motion at a site from the prediction of the GMPE at hand, we couple the 1D soil amplification resulting from equivalent-linear ground-response analyses (Mascandola et al., 2021) with the 3D basin amplification quantified by the δ_{bas} term of the regional ground-motion attenuation model of Lanzano et al. (2016). While the 1D amplification is incorporated into the hazard through the convolution method of Bazzurro and Cornell (2004), following the upgrade of Barani and Spallarossa (2017), the 3D amplification is directly incorporated into the rock GMPE selected for the present application. The methods are described in the sections below and the computational workflow is schematized in Figure 2.

Incorporation of 1D Amplification

The convolution method (Bazzurro and Cornell, 2004; Barani and Spallarossa, 2017) computes the surface hazard curve at the site of interest by convolving two probability distributions. The former is defined by the hazard curve on rock (which is here amended with the δ_{bas} term; see next section), and the latter is the probability distribution of site amplification, which is expressed by a period-dependent amplification function $AF(T)$ defined as the ratio of the spectral acceleration at the surface to the spectral acceleration at the (outcropping) bedrock. The amplification functions for all computation nodes are shown in Figure 3. It can be observed that they identify two main trends (for further details, interested readers may refer to the original article of Mascandola et al. (2021)), demarcating two sectors of the Po Plain: one set of functions is peaked around 1 s (dark gray curves in Figure 3) and corresponds to the nodes in the northwestern and central sectors of the study area (dark gray dots in Figure 1a); the other set presents a flatter trend (light gray curves in Figure 3) and corresponds to the nodes in the southeastern sector of the plain (light gray dots in Figure 1a).

For a given soil profile, predictive models for $AF(T)$, also termed as Soil Amplification Predictive Equations (SAPEs), can be determined by regression of $AF(T)$ versus the spectral acceleration on rock, $Sa_r(T)$. Following Rodriguez-Marek et al. (2014), we adopt a linear model represented by the equation below:

$$\log AF(T) = c_1 + c_2 \log Sa_r(T) + \varepsilon_{\log AF(T)} \qquad (3)$$

where c_1 and c_2 are regression coefficients, and $\varepsilon_{\log AF(T)}$ is the Gaussian residual with zero mean and standard deviation $\sigma_{\log AF(T)}$.

Following Bazzurro and Cornell (2004), we assume that $AF(T)$ is drawn from a log-normal distribution, whose mean and standard deviation are defined by the SAPE of the soil profile of interest. Hence, one can easily obtain the probability of exceeding a given amplification level conditioned to a certain value of the spectral acceleration on rock.

The surface hazard curve (i.e., the annual probability of exceeding the ground-motion level z at the surface) is calculated as:

$$G_Z(z) = \sum_{x_j} P\left[AF(T) > \frac{z}{x_j} | x_j\right] p_X(x_j) \qquad (4)$$

where $P\left[AF(T) > \frac{z}{x_j} | x_j\right]$ is the probability that $AF(T)$ is greater than $\frac{z}{x_j}$ given that the rock ground-motion level is x_j, and $p_X(x_j)$ is the annual probability of occurrence of $X = x_j$ (which can be obtained by differentiating the rock hazard curve).

In order to account for the epistemic uncertainty in ground response, for each node of the grid in Figure 1a, Mascandola et al. (2021) applied a Monte Carlo simulation procedure that randomly varies the values of the soil properties considered in the 1D numerical modelling (one hundred randomizations were performed). Specifically, for each layer of each soil model, the uncertainty affecting thickness, shear wave velocity, and in shear modulus reduction and damping ratio curves was considered.

While the original method of Bazzurro and Cornell (2004) computes a single SAPE from a set of *n* Monte Carlo realizations of the soil model at the base of which *k* accelerograms are driven, here we define *n* = 100 SAPEs (Figure 4a) – one for each Monte Carlo realization (Figure 4b) – for each computation node according to Barani and Spallarossa (2017). In that study, the authors have shown that the original approach of Bazzurro and Cornell (2004) mixes the input motion variability and the uncertainty in the parameters of the soil model, which are both reflected in the value of $\sigma_{\log AF(T)}$. While the former has a pure aleatoric nature, the latter is mainly epistemic. In order to separate epistemic and aleatoric contributions, Barani and Spallarossa (2017) proposes to determine a SAPE for each one of the *n* randomized soil models at the base of which *k* accelerograms are driven. This leads to a set of *n* SAPEs (Figure 4a), each of which is then used in the convolution calculations, thus producing a bundle of site-specific hazard curves at each investigated site (see Figure 2). Besides the correct separation and representation of epistemic and aleatoric contributions, this approach has also the advantage of avoiding the over-smoothing of the amplification curves, which occurs when one averages the amplification functions obtained from *n* soil samples. Ulmer et al. (2021) have shown that the over-smoothing of the amplification curves could lead to decreased hazard as the epistemic uncertainty increases. Moreover, compared to the logic tree approach to manage the epistemic uncertainty in soil models (e.g., Rodriguez-Marek et al., 2021), it avoids assigning subjective weights to the alternative assumptions considered. Indeed, weights are implicitly assigned in the Monte Carlo simulation when sampling the probability density functions associated with the uncertain soil parameters. Most realizations of the random process are concentrated around the mean of each probability density function and only few extreme (low likelihood) values are sampled.

It is worth noting that, using the procedure of Barani and Spallarossa (2017), $\sigma_{\log AF(T)}$ represents the aleatory variability of the seismic amplification due to the record-to-record variability at the site of interest. This variability is already included in the ϕ_{SS} term (Equation 1 and Equation 2) except for significant soil non-linearity (Abrahamson personal comm., 2022). Indeed, ϕ_{SS} is generally dominated by data in the linear range. In the case of substantial soil non-linearity, additional variance from the non-linear effects should be considered in the total ground-motion sigma. For medium-to-long spectral periods, on which we focus here, Mascandola et al. (2021) found mild non-linear effects. Therefore, we set $\sigma_{\log AF(T)}$ to zero, so as to avoid double counting of the same component of the ground-motion variability.

Incorporation of 3D Amplification

The basin-related amplification is considered here through the δ_{bas} term included in the regional ground-motion attenuation model of Lanzano et al. (2016). This term is a period-dependent, spatially invariant, amplification factor (black line in Figure 3) that quantifies the average influence of the 3D amplification in the Po Plain area and surrounding. The δ_{bas} term takes into account the amplification due to the trapping and conversion of body waves in the thick sedimentary cover above the basin-shaped basement. Such phenomena are responsible for the generation of surface waves that dominate the seismic signals, especially at longer periods (e.g., Luzi et al., 2013; Lanzano et al., 2016). Conversely, in the short-period range (T < 1 s), the δ_{bas} term tends to de-amplify the ground shaking, possibly because of the strong attenuation of the short-period waves propagating through the thick sedimentary cover (Lanzano et al., 2016).

For computational purposes, the δ_{bas} term is included in the PSHA by amending the GMPE for rock conditions (i.e., $V_{S,30} \geq 800\ m/s$) selected for the present application (see next section). Mathematically, the mean value of the (logarithmic) spectral acceleration at the site of interest, $Sa_{\delta_{bas}}(T)$, is calculated as:

$$\log Sa_{\delta_{bas}}(T) = \log Sa_r(T) + \delta_{bas}(T) \qquad (5)$$

where $\log Sa_r(T) = f(M, R, \theta)$ indicates the mean (logarithmic) spectral acceleration on rock predicted by the GMPE as a function of magnitude (M), distance (R), and other parameters θ (e.g., source mechanism).

The uncertainty associated with the δ_{bas} term ($\sigma_{\delta_{bas}}$), which is accounted for via logic tree (see next section), is computed from the values of the $\delta S2S_s$ site term provided by Lanzano et al. (2017) for a subset of accelerometric stations selected among those considered by Lanzano et al. (2016). Specifically, under the assumption that the 1D and 3D amplifications are uncorrelated random variables (or mildly correlated), we computed $\sigma_{\delta_{bas}}$ by removing the contribution related to the 1D soil amplification, σ_{1D}, from the standard deviation of $\delta S2S_s$, $\phi_{S2S-PoPlain}$, namely:

$$\sigma_{\delta_{bas}} = \sqrt{\phi^2_{S2S-PoPlain} - \sigma^2_{1D}} \qquad (6)$$

where σ_{1D} is computed as

$$\sigma_{1\mathrm{D}} = \sqrt{\frac{\sum_{i=1}^{N_S}\left(\log AF(T)_i - \mu_{\log AF(T)}\right)^2}{N_S - 1}} \qquad (7)$$

In the equation above, N_S indicates the number of computation nodes (Figure 1a), $AF(T)_i$ is the amplification function associated with the *i*-th node (Figure 3) resulting from the 1D equivalent linear ground-response analysis (Mascandola et al., 2021), and $\mu_{\log AF(T)}$ is the mean logarithmic amplification function. Note that the values of $AF(T)_i$ are average values computed over *n* by *k* samples.

All terms in Equation (6) are displayed in Figure 5, along with the site-to-site variability ($\phi_{S2S-NI15}$) associated with the regional GMPE for Northern Italy of Lanzano et al. (2016). Note that the values of $\phi_{S2S-PoPlain}$ and, in turn, those of $\sigma_{\delta_{bas}}$ are affected by the source ground-motion dataset (i.e., by its completeness), which is dominated by recordings from earthquakes belonging to a limited number of sources. About 70% of the records in the dataset used by Lanzano et al. (2017) belong to the 2012 Emilia sequence. Hence, most stations in the dataset (54%) sample one main source-to-site path. In addition, their distribution over the Po Plain region is uneven, with a greater concentration in the central-eastern sector, where several temporary stations were installed during the 2012 Emilia sequence. Finally, about 1/3 of the stations show a limited number of recordings, between 5 and 10. Last but not least, it is worth noting that σ_{1D} only accounts for the variability in the 1D site response associated with the soil layers above the seismic bedrock. Hence, $\sigma_{\delta_{bas}}$ may also incorporate to some extent the contribution to site response associated with deeper discontinuities (Mascandola et al., 2019), which is implicitly captured by $\phi_{S2S-PoPlain}$.

Hazard Computation: Logic Tree and Basic Assumptions

The hazard computations are carried out through the conventional Cornell source-based approach (Cornell, 1968), considering the source-zone model developed by Santulin et al. (2017) for the updated seismic hazard map of Italy (Meletti et al., 2021) (details relative to seismogenic zones are described in the electronic supplement). A single GMPE is adopted, the ITA18 model recently proposed by Lanzano et al. (2019) for shallow crustal earthquakes in Italy. The selection of this model was guided by two main criteria: (1) all GMPEs for Italy have been superseded by ITA18; (2) compared to previous models, including the regional one for Northern Italy of Lanzano et al. (2016), the magnitude range of applicability of ITA18 is fully consistent with the $M_{\min} - M_{\max}$ range covered by the source-zone parameterization (see the electronic supplement). Finally, the seismic hazard curves (i.e., the probability of exceeding certain ground motion values in a given time period) are calculated assuming that seismicity follows a Poisson process.

Given the scope of the study, which focuses on the incorporation and impact of site-response on the hazard, our study does not account for the epistemic uncertainty affecting the earthquake sources and the related recurrence model. Hence, a simple logic tree is adopted, and only the uncertainties affecting the assumptions related to ground-motion characterization are considered (Figure 6).

The requirements to apply a partially non-ergodic PSHA approach imply that both the epistemic uncertainty in site amplification and the epistemic uncertainty in the single-station standard deviation must be taken into account. While the epistemic uncertainty in the 1D site response is considered by using multiple SAPEs (see previous section), the epistemic uncertainty in the 3D amplification is modeled via a three-point discrete approximation to a normal distribution (Keefer and Bodily, 1983).

A discrete distribution with values of $\delta_{bas} + 1.645\sigma_{\delta_{bas}}$, δ_{bas}, $\delta_{bas} - 1.645\sigma_{\delta_{bas}}$ is assumed. Computationally, this is reflected in the use of a simple logic tree with three branches (Figure 6) with weights of 0.63 on the median model and weights of 0.185 on the 5th and the 95th percentiles (±1.645 standard deviations).

Concerning the epistemic uncertainty in the single-station standard deviation, we model the uncertainty associated with the ϕ_{SS} term. Again a three-point discrete distribution is considered, with values of $\phi_{SS} + 1.645\sigma_{\phi_{SS}}$, ϕ_{SS}, $\phi_{SS} - 1.645\sigma_{\phi_{SS}}$, where $\sigma_{\phi_{SS}} = 0.1 \times \phi_{SS}$ is the standard deviation of ϕ_{SS}. We adopt here a coefficient of variation for ϕ_{SS} equal to 0.1 according to Rodriguez-Marek et al. (2014).

Finally, we consider the epistemic uncertainty in the median ground-motion prediction, which may be related to the limited data in the original ground-motion data set and over-simplifications in the parameterization of propagation and attenuation effects (e.g., Al Atik and Youngs, 2014). This uncertainty is quantified by the standard deviation of the mean (logarithmic) ground motion, σ_μ. Once again, a three-point discrete approximation to a normal distribution is considered to model this source of epistemic uncertainty (Figure 6).

Altogether, the logic tree (Figure 6) consists of 27 paths corresponding to 27 computation runs that are repeated for each node of the grid in Figure 1a for each period of interest. For each period, the resulting 27 hazard curves are then convolved with the corresponding 100 SAPEs obtained from the ground-response analysis (last step in the diagram in Figure 2).

Results

The maps in Figure 7 display the mean site-specific hazard estimates corresponding to a return period of 475 years for the entire study area. We present maps for Peak Ground Acceleration, PGA, and spectral acceleration, $Sa(T)$, corresponding to 1 s (1 Hz), 1.6 s (0.6 Hz), and 3 s (0.3 Hz). Although the numerical soil models used in the ground-response analysis lack detail on minor, shallower discontinuities, which is reflected in the lack of resolution at higher frequencies, we also present the PGA map. Indeed, deep soil discontinuities have a larger impact on lower frequencies (e.g., Inzunza et al., 2019), but can also affect high-frequency ground motion (Yamanaka et al., 2012; Zhu et al., 2020). The other spectral periods are chosen according to the frequency range where amplification effects due to the soft sediments above the seismic bedrock have been observed (Mascandola et al., 2019 and 2021). For comparison purposes, $V_{S,30}$-driven ergodic hazard maps corresponding to the same return period of 475 years are shown in Figure 8. They were simply obtained by running the hazard computations using the ITA18 GMPE with its own site term, $F_S(V_{S,30})$. No correction for 3D amplification and no source of epistemic uncertainty are considered in this case. The values of $V_{S,30}$ taken as reference are those mapped by Forte et al. (2019).

The comparison between Figure 7 and Figure 8 highlights the improvements achieved by applying a partially non-ergodic approach based on site-specific ground response characterization instead of a more conventional, albeit simpler, method which accounts for site amplification through a generic correction term based on $V_{S,30}$. The two methods provide consistent results in terms of spatial distribution of the hazard, which shows a general increase towards south-east due to the greater contribution of certain seismogenic zones characterized by a higher seismicity (especially, zone #513, #517, and #519; see Figure S1 in the electronic supplement). However, except for a few areas (i.e., towards the Garda Lake, near Reggio-Emilia, Bologna, and north-east of Ferrara) where 1D soil amplification was found to be greater (Mascandola et al., 2021), the approach adopted here (Figure 7) provides lower hazard values compared to the simpler ergodic method (Figure 8), with differences up to -50% (Figure 9). We recall here that the values of the ergodic sigma are greater than those of the partially non-ergodic counterpart, thus producing higher hazard values. Nevertheless, the maps in Figure 7 provide a finer picture of the hazard, highlighting those areas where the ground-motion hazard is actually dominated by local amplification effects. As the δ_{bas} term is spatially invariant, this is attributable to the spatial variability of the 1D amplification (Figure 3) which, in turn, can be related to regional variations in the depth of the seismic bedrock (Mascandola et al., 2019) and shear-wave velocity of the soft sediments above it (Mascandola et al., 2021). For instance, analyzing the PGA map (Figure 7a), the zone with the highest hazard is around Reggio-Emilia, where the PGA values are between 0.225 and 0.250 g. This zone is located at the junction between the Ferrara-Romagna Arc (seismogenic zone #519 in Figure S1 of the electronic supplement) and the Emilia Arc (which traverses zones #513 and #517 in Figure S1), an area where the hazard on rock is at higher levels (Figure S2 in the electronic supplement) and the seismic bedrock is shallower (around 150 m deep (Mascandola et al., 2019)), thus affecting the ground response at shorter periods (< 1.4 s; Figure 7a). In the other sectors of the plain, the PGA hazard tends to follow the trend of the active buried thrusts (e.g., the Ferrara-Romagna Arc in Figure 1a), with higher values (up to 0.2 g) near the top of the main anticlines (source zone #519 in Figure S1 of the electronic supplement) where, again, amplification effects at shorter periods (< 1.2 s) have been observed (Figure 7a). Lower PGA values (around 0.100-0.150 g) can be observed in the inner part of the Ferrara-Romagna thrust front, between Reggio-Emilia and Bologna, where the seismic bedrock is deeper (Mascandola et al., 2019). The PGA for the return period considered decreases significantly toward the center of the basin (particularly towards the eastern and western edges), where no seismogenic zones were defined (Figure S1) and increases further north towards the Garda Lake (see Figure 1a), in correspondence of the source zone #102 (Figure S1 in the electronic supplement). The site-specific hazard maps for spectral acceleration (Figure 7 b-d) display patterns similar to the PGA map for the same return period (Figure 7a). However, the highest hazard values move to the southeastern sector of the map, where the deeper seismic bedrock and the lower shear-wave velocities in the soil cover (Figure 1b) contribute to the amplification at longer periods. Note that this trend in the hazard values nearly reflects the grouping of the computation nodes shown in Figure 1a (which is based on the grouping of the amplification curves in Figure 3), with dark gray nodes to the north presenting amplification functions peaked around 1 s and light gray nodes to the southeast showing greater amplification at longer periods (i.e., > 1 s).

Uncertainty and Sensitivity Analysis

The epistemic uncertainty in the hazard results, which is quantified by the spread (i.e., difference) between the ground-motion values corresponding to the 84th and 16th percentiles ($\Delta_{84\text{-}16}$) of the distribution of the ground motion for the 475-year return period, is shown in Figure 10 for the four response periods considered. On average, the maps show that $\Delta_{84\text{-}16}$ increases according to the general increase of the mean site-specific hazard (see Figure 7). The uncertainty is greater for $Sa(1\ s)$ (Figure 10b) and decreases significantly at longer periods (Figure 10c-d). This effect is mainly attributable to the uncertainty affecting ϕ_{SS} (we recall that $\sigma_{\phi_{SS}} = 0.1 \times \phi_{SS}$), which for small-to-moderate magnitudes ($M_w < 6$) – those contributing mostly to the hazard (Mascandola et al., 2020) – tends to decrease with increasing period (Figure 11a), while both $\sigma_{\delta_{bas}}$ (Figure 5) and σ_{μ} (Figure 11b) are fairly constant. This is in agreement with the results of Rodriguez-Marek et al. (2013) showing a similar behavior for the ϕ_{SS} parameter.

To evaluate the sensitivity of the hazard and its uncertainty to the 3D and 1D amplification, we repeated the hazard analysis removing the contribution of the δ_{bas} term and 1D amplification one at a time. Then, for each ground-motion parameter of interest and for each node of the computation grid (Figure 1a), we computed the value of $\Delta_{84\text{-}16}$. The sensitivity of the hazard and its uncertainty is shown by the boxplots in Figure 12. Again, we refer to a return period of 475 years. Specifically, for the entire study area (i.e., all computation nodes together), Figure 12a shows the percentage change in the mean hazard when the 3D amplification is neglected, while the contribution of the uncertainties affecting the 1D and 3D amplification to the final hazard (expressed by $\Delta_{84\text{-}16}$) is shown in Figure 12b. Figure 12a reveals that neglecting the contribution of the δ_{bas} term leads to significant hazard underestimations (~ 30%) at medium-to-long spectral periods, while overestimations of about 10% can be observed for the PGA. As is clear from Figure 3, this effect is attributable to the δ_{bas} term, which tends to amplify the ground motion in the long-period range ($T > 1$s) and to decrease it at shorter periods.

Concerning the effects on the hazard uncertainty, Figure 12b indicates that the δ_{bas} term is the parameter that contributes the most to it, reflecting our poor knowledge of basin effects in the study area. Specifically, it contributes about 60% to 80% to the total hazard uncertainty for all periods considered, while the epistemic uncertainty in 1D amplification contributes about 20%. It follows that the remaining contribution to the hazard uncertainty, which is related to the uncertainty in ϕ_{SS} and σ_{μ}, is less than a 20%. It is smaller at longer spectral periods (< 10%) and greater for the PGA (~ 20%).

Similar considerations can be drawn by analyzing Figure 13, which shows the Uniform Hazard Spectra (UHSs) for a return period of 475 years, with and without the contribution of the δbas term, for four main cities (Milano, Bologna, Reggio Emilia, and Ferrara) located in areas with different seismic hazard (Figure 7). Among these sites, Milano shows the lowest hazard level. This city is in a very low seismicity area, which is not covered by any source zone (see Figure S1 in the electronic supplement). Hence, its hazard is controlled by strong, distant events (e.g., Barani et al., 2009). On the other hand, the hazard at the other selected cities is mostly controlled by the local seismicity (i.e., nearby source zones). Again, one can observe that neglecting the contribution associated with basin effects (i.e., the δ_{bas} term) leads to significant hazard underestimations at medium-to-long spectral periods, while a minor overestimation can be observed at shorter periods. Moreover, it is again evident that the uncertainty related to such basin effects is the major contributor to the total hazard uncertainty.

Conclusions

We have presented a probabilistic seismic hazard analysis for the entire Po Plain sedimentary basin in Northern Italy, an area that poses a significant challenge because of its strategic relevance related to the high population density and numerous infrastructures, as well as the geological setting, which is responsible for significant amplifications in the long-period range. Furthermore, its extension makes the Po Plain one of the widest Quaternary alluvial basins in Europe, thus entailing a considerable effort for the in-depth knowledge of the seismic response and, consequently, the seismic hazard.

This study has focused on the incorporation of seismic amplification into the PSHA, including the analysis of the sensitivity of the hazard and its uncertainty to the 1D and 3D amplification, which are both considered in the computations. While the 1D amplification was estimated through equivalent-linear ground-response analysis (Mascandola et al., 2021) and was then incorporated into the hazard via the Approach 3 of the U.S. Nuclear Regulatory Commission, 3D basin effects were considered through the application of an empirical correction term (Lanzano et al., 2016) to the median rock ground motion predicted by the attenuation model considered in the PSHA. The hazard assessment was carried out by applying the single-station sigma approach.

Compared to simpler approaches that rely on rough site classification schemes (e.g., based on $V_{S,30}$), the approach adopted in the present study, albeit seemingly complex, has been found to provide a finer picture of the seismic hazard, highlighting those areas where the ground motion is actually affected by local amplification effects due to local or regional geological features. Actually, the complexity of the approach depends only on the amount of data needed for the ground response assessment, especially on a regional scale. Depending on data availability, the convolution approach can be easily applied to other regions worldwide, in favor of more refined hazard mapping.

The sensitivity analysis has revealed that neglecting basin effects leads to significant underestimation of the hazard (about 30% for a return period of 475 years), especially at longer spectral periods (> 1s). Moreover, our poor knowledge of basin effects has been found to be the main contributor to the total epistemic uncertainty in the results, while the uncertainty in the 1D site-response characterization contributes for a minor proportion (~ 20%). Therefore, in order to reduce the epistemic uncertainty in the hazard, further efforts are needed to improve the characterization of basin effects. To this end, future developments may include the application of spatial correlation models of ground motion with spatially correlated site terms (e.g., Rahpeyma et al., 2018; Sgobba et al., 2019;

Menafoglio et al. 2020) or the incorporation of amplification functions from 3D physics-based numerical simulations (e.g., Smerzini et al., 2017). As new data will become available, they will help improve the hazard both at high frequencies, through the incorporation of shallower discontinuities in the soil model, and at very low frequencies, through the modeling of the geologic bedrock, at the expense of increased complexity of the computation model. The latter should include all potential sources of epistemic uncertainty affecting both the rock hazard (e.g., uncertainty in seismic sources, recurrence model, maximum magnitude value) and site-response characterization (e.g., site-to-site variability of target site conditions and high-frequency attenuation (e.g., Al Atik et al., 2014; Rodriguez-Marek et al., 2014; Ameri et al., 2017; Aristazabal et al., 2022)), and propagate them through to the final hazard result.

Data and Resources

The basic input data used in the hazard assessment are described in the Supplemental Material along with ergodic hazard maps for rock conditions. The Parametric Catalogue of Italian Earthquakes (CPTI15) is openly available at: https://emidius.mi.ingv.it/CPTI15-DBMI15/download_CPTI15.htm. The Database of Individual Seismogenic Sources (DISS) is available at: https://diss.ingv.it/ . All websites were last accessed in August 2022.

Declaration of Competing Interests

The authors acknowledge there are no conflicts of interest recorded.

Acknowledgments

We are grateful to Norman A. Abrahamson for his suggestions on the treatment of uncertainties in the hazard assessment, and Giovanni Lanzano for the fruitful discussions about the use of δ_{bas} and the quantification of its uncertainty. Last but not least, we express our gratitude to Jacopo Jiritano

(Quantectum Earthquake Forecast Center), who contributed to the calculation of the values of the coefficients of the Gutenberg and Richter relation in the initial stages of the work. We are grateful to the Associate Editor, Céline Beauval, and two anonymous reviewers for their suggestions that brought significant improvements to the study.

References

Abraham, J.R., Lai, C.G., and Papageorgiou, A. (2015). Basin-effects observed during the 2012 Emilia earthquake sequence in Northern Italy. Soil Dynamics and Earthquake Engineering, 78, 230-242.

Al Atik L., Kottke A., Abrahamson N., and Hollenback J. (2014). Kappa (κ) scaling of ground-motion prediction equations using an inverse random vibration theory approach. Bulletin of the Seismological Society of America, 104, 336-346.

Al Atik, L., Abrahamson, N., Cotton, F., Scherbaum, F., Bommer, J.J., and Kuehn, N. (2010). The variability of ground-motion prediction models and its components. Seismological Research Letters, 81 (5), 794-801.

Al Atik, L., and Youngs, R.R. (2014). Epistemic uncertainty for NGA-West2 models. Earthquake Spectra, 30(3), 1301-1318.

Ameri G., Hollender F., Perron V., and Martin C. (2017). Site-specific partially nonergodic PSHA for a hard-rock critical site in southern France: adjustment of ground motion prediction equations and sensitivity analysis. Bulletin of Earthquake Engineering, 15, 4089-4111.

Ameri, G., Massa, M., Bindi, D., D'Alema, E., Gorini, A., Luzi, L., Marzorati, S., Pacor, F., Paolucci, R., Puglia, R., and Smerzini, C. (2009). The 6 april 2009, Mw 6.3, L'Aquila (Central Italy) earthquake: strong-motion observations. Seismological Research Letters, 80 (6), 951-966.

Anderson, J.G., and Brune J.N. (1999). Probabilistic seismic hazard analysis without the ergodic assumption. Seismological Research Letters, 70(1), 19-28.

Aristizabal, C., Bard, P.Y., and Beauval, C. (2022). Site-Specific PSHA: Combined Effects of Single-Station-Sigma, Host-to-Target Adjustments and Nonlinear Behavior. A case study at Euroseistest. Italian Journal of Geosciences, 141(1), 5-34.

Atkinson, G.M. (2006). Single-station sigma, Bull. Seismol. Soc. Am. 96, 446-455.

Barani, S., and Spallarossa, D. (2017). Soil amplification in probabilistic ground motion hazard analysis. Bulletin of Earthquake Engineering, 15(6), 2525-2545.

Barani, S., Ferretti, G., and De Ferrari, R. (2020). Incorporating results from seismic microzonation into probabilistic seismic hazard analysis: An example in western Liguria (Italy). Engineering Geology, 267, 105479.

Barani, S., Spallarossa, D., and Bazzurro, P. (2009). Disaggregation of Probabilistic Ground-Motion Hazard in Italy. Bulletin of the Seismological Society of America, 99(5), 2638-2661.

Bazzurro, P. (1998). Probabilistic seismic demand analysis. Ph.D. Thesis, Stanford University, Palo Alto, CA.

Bazzurro, P., and Cornell, C.A. (2004). Nonlinear Soil-Site Effects in Probabilistic Seismic-Hazard Analysis Bulletin of the Seismological Society of America, 94(6), 2110-2123.

Bradley, B.A. (2012). Ground motions observed in the Darfield and Christchurch earthquakes and the importance of local site response effects. New Zealand journal of geology and geophysics, 55(3), 279-286.

Burrato, P., Vannoli, P., Fracassi, U., Basili, R., and Valensise, G. (2012). Is blind faulting truly invisible? Tectonic-controlled drainage evolution in the epicentral area of the May 2012, Emilia-Romagna earthquake sequence (northern Italy). Annals of Geophysics.

Carminati, E., and Doglioni, C. (2012). Alps vs. Apennines: The paradigm of a tectonically asymmetric Earth. Earth-Science Reviews, 112(1-2), 67-96.

Cornell, C. A. (1968). Engineering Seismic Risk Analysis. Bulletin of the Seismological Society of America, 58(5), 1583-1606.

Cornell, C.A. (1968). Engineering seismic risk analysis. Bull. Seismol. Soc. Am. 58, 1583-1606.

Cornell, C.A., and Vanmarcke, E.H. (1969). The major influences on seismic risk. In Proceedings of the fourth world conference on earthquake engineering, Chilean Assoc. on Seismol. and Earthquake Eng., Santiago, Chile, vol. 1, pp. 69-83.

Cramer, C. H., Gomberg, J. S., Schweig, E. S., Waldron, B. A., and Tucker, K. (2006). First USGS urban seismic hazard maps predict the effects of soils. Seismological Research Letters, 77(1), 23-29.

Cramer, C. H., Gomberg, J. S., Schweig, E. S., Waldron, B. A., and Tucker, K. (2004). The Memphis, Shelby County, Tennessee, Seismic Hazard Maps. US Geological Survey Open-File Report, 4, 1294.

Cramer, C. H., Van Arsdale, R. B., Dhar, M. S., Pryne, D., and Paul, J. (2014). Update of Urban Seismic- Hazard Maps for Memphis and Shelby County, Tennessee: Geology and VS Observations. Seismological Research Letters, 85(5), 986-996.

Cramer, C.H. (2006). Quantifying the uncertainty in site amplification modeling and its effects on site-specific seismic-hazard estimation in the upper Mississippi embayment and adjacent areas. Bulletin of the Seismological Society of America, 96(6), 2008-2020.

DISS Working Group (2015). Database of individual seismogenic sources (DISS), Version 3.2.0: A compilation of potential sources for earthquakes larger than M 5.5 in Italy and surrounding areas. http://diss.rm.ingv.it/diss/, © INGV 2015 - Istituto Nazionale di Geofisica e Vulcanologia.

Doglioni, C. (1993). Some remarks on the origin of foredeeps, Tectonophysics, 228(1-2), 1-20.

European Committee for Standardization (2004). Eurocode 8: design of structures for earthquake resistance. P1: General rules, seismic actions and rules for buildings. Draft 6, Doc CEN/TC250/SC8/N335.

Faccioli, E., Paolucci, R., and Vanini, M. (2015). Evaluation of probabilistic site-specific seismic-hazard methods and associated uncertainties, with applications in the Po Plain, Northern Italy. Bull. Seismol. Soc. Am. 105, 2787-2807.

Felicetta, C., Mascandola, C., Spallarossa, D., Pacor, F., Hailemikael, S., and Di Giulio, G. (2021). Quantification of site-effects in the Amatrice area (Central Italy): Insights from ground-motion recordings of the 2016–2017 seismic sequence. Soil Dynamics and Earthquake Engineering, 142, 106565.

Forte, G., Chioccarelli, E., De Falco, M., Cito, P., Santo, A., and Iervolino, I. (2019). Seismic soil classification of Italy based on surface geology and shear-wave velocity measurements. Soil Dynamics and Earthquake Engineering, 122, 79-93.

Inzunza D. A., Montalva G. A., Leyton F., Prieto G., and Ruiz S. (2019). Shallow ambient- noise 3D tomography in the Concepción Basin, Chile: implications for low- frequency ground motions. Bulletin of the Seismological Society of America, 109(1), 75-86.

Kato, B., and Wang, G. (2021). Regional seismic responses of shallow basins incorporating site- city interaction analyses on high- rise building clusters. Earthquake Engineering & Structural Dynamics, 50(1), 214-236.

Keefer, D. L., and Bodily, S. E. (1983). Three-point approximations for continuous random variables. Management Science, 29(5), 595-609.

Lai, C.G., Poggi, V., Famà, A., Zuccolo, E., Bozzoni, F., Meisina, C., Bonì, R., Martelli, L., Massa, M., Mascandola, C., Petronio, L., Affatato, A., Baradello, L., Castaldini, D., and Cosentini, R. M. (2020). An inter-disciplinary and multi-scale approach to assess the spatial variability of ground motion for seismic microzonation: the case study of Cavezzo municipality in Northern Italy. Engineering geology, 274, 105722.

Lanzano, G., D’Amico, M., Felicetta, C., Puglia, R., Luzi, L., Pacor, F., and Bindi, D. (2016). Ground- motion prediction equations for region- specific probabilistic seismic- hazard analysis. Bulletin of the Seismological Society of America, 106(1), 73-92.

Lanzano, G., Luzi, L., Pacor, F., Felicetta, C., Puglia, R., Sgobba, S., and D'Amico, M. (2019), A revised ground- motion prediction model for shallow crustal earthquakes in Italy, Bull. Seis. Soc. Am., 109 (2), 525-540.

Lanzano, G., Pacor, F., Luzi, L., D'amico, M., Puglia, R., and Felicetta, C. (2017). Systematic source, path and site effects on ground motion variability: the case study of Northern Italy. Bulletin of Earthquake Engineering, 15(11), 4563-4583.

Lin, P. S., Chiou, B., Abrahamson, N.A., Walling, M., Lee, C. T., and Cheng, C. T. (2011). Repeatable source, site, and path effects on the standard deviation for empirical ground-motion prediction models. Bulletin of the Seismological Society of America, 101(5), 2281-2295.

Luzi, L., Pacor, F., Ameri, G., Puglia, R., Burrato, P., Massa, M., Augliera, P., Franceschina, G., Lovati, S., and Castro, R. (2013). Overview on the strong- motion data recorded during the May–June 2012 Emilia seismic sequence. Seismological Research Letters, 84(4), 629-644.

Martelli, L., and Ercolessi, G. (2020). Evaluation and representation of the local seismic hazard through the H MS parameter: example in Emilia-Romagna. Bollettino di Geofisica Teorica ed Applicata, 61(1).

Martelli, L., and M. Romani (2013). Microzonazione Sismica e analisi della condizione limite per l'emergenza delle aree epicentrali dei terremoti della pianura emiliana di maggio-giugno 2012, relazione illustrativa, Servizio geologico, sismico e dei suoli Regione Emilia Romagna (in Italian).

Martelli, L., Bonini, M., Calabrese, L., Corti, G., Ercolessi, G., Molinari, F. C., Piccardi, L., Pondrelli, S, Sani, F., and Severi, P. (2017). Carta sismotettonica della Regione Emilia-Romagna e aree limitrofe, scala 1:250.000 (edizione 2016), Con note illustrative, Regione Emilia-Romagna, SGSS; CNR, IGG sez. FI; Università degli Studi di Firenze, DST; INGV sez. BO. D.R.E.AM., Italy (in Italian).

Mascandola, C., Barani, S., Massa, M., and Albarello, D. (2021). New insights into long- period (> 1 s) seismic amplification effects in deep sedimentary basins: A case of the Po Plain basin of northern Italy. Bulletin of the Seismological Society of America, 111(4), 2071-2086.

Mascandola, C., Barani, S., Massa, M., Paolucci, E., and Albarello, D. (2020). Clustering analysis of probabilistic seismic hazard for the selection of ground motion time histories in vast areas. Bulletin of Earthquake Engineering, 18(7), 2985-3004.

Mascandola, C., Massa, M., Barani, S., Albarello, D., Lovati, S., Martelli, L., and Poggi, V. (2019). Mapping the Seismic Bedrock of the Po Plain (Italy) through Ambient- Vibration Monitoring. Bulletin of the Seismological Society of America, 109(1), 164-177.

Mascandola, C., Massa, M., Barani, S., Lovati, S., Santulin, M. (2017). Long-period amplification in deep alluvial basins and consequences for site-specific probabilistic seismic hazard analysis: an example from the Po Plain (Northern Italy). Bull. Seismol. Soc. Am. 107, 770786.

Massa, M., Barani, S., and Lovati, S. (2014). Overview of topographic effects based on experimental observations: meaning, causes and possible interpretations. Geophysical Journal International, 197(3), 1537-1550.

McGuire, R.K., Silva, W. J., and Costantino, C. J. (2001). Technical basis for revision of regulatory guidance on design ground motions: Hazard and risk-consistent ground motion spectra guidelines, in NUREG/CR-6728, U.S. Nuclear Regulatory Commission, Washington D.C.

Meletti C., Marzocchi, W., D'Amico, V., Lanzano, G., Luzi, L., Martinelli, F., Pace, B., Rovida, A., Taroni, M., Visini F., and the MPS19 Working Group (2021), The new Italian Seismic Hazard Model (MPS19), Annals of Geophysics, 64, 1, SE112, 2021, doi:10.4401/ag-8579

Menafoglio, A., Sgobba, S., Lanzano, G., and Pacor, F. (2020). Simulation of seismic ground motion fields via object-oriented spatial statistics with an application in Northern Italy. Stochastic Environmental Research and Risk Assessment, 34(10), 1607-1627.

Meroni, F., Squarcina, T., Pessina, V., Locati, M., Modica, M., and Zoboli, R. (2017). A damage scenario for the 2012 Northern Italy Earthquakes and estimation of the economic losses to residential buildings. International Journal of Disaster Risk Science, 8(3), 326-341.

Ministero delle Infrastrutture e dei Trasporti (2018). Aggiornamento delle Norme Tecniche per le Costruzioni. Part 3.2.2: Categorie di sottosuolo e condizioni topografiche, Gazzetta Ufficiale n. 42 del 20 febbraio 2018 (in Italian).

Moczo, P., Kristek, J., Bard, P. Y., Stripajová, S., Hollender, F., Chovanová, Z., Kristeková M., and Sicilia, D. (2018). Key structural parameters affecting earthquake ground motion in 2D and 3D sedimentary structures. Bulletin of Earthquake Engineering, 16(6), 2421-2450.

Muttoni, G., C. Carcano, E. Garzanti, M. Ghielmi, A. Piccin, R. Pini, S. Rogledi, and D. Sciunnach (2003). Onset of major Pleistocene glaciations in the Alps, Geology, 31(11): 989-992.

Pieri, M., and G. Groppi (1981). Subsurface geological structure of the Po Plain, Italy, in Progetto Finalizzato Geodinamica/Sottoprogetto "Modello Strutturale", edited by C.N.R., Publ. N° 414.

Rahpeyma, S., Halldorsson, B., Hrafnkelsson, B., and Jónsson, S. (2018). Bayesian hierarchical model for variations in earthquake peak ground acceleration within small- aperture arrays. Environmetrics, 29(3), 1- 19.

Rodriguez-Marek A., Cotton F., Abrahamson N. A., Akkar S., Al Atik L., Edwards B., Montalva G. A., and Dawood H. M. (2013). A model for single-station standard deviation using data from various tectonic regions. Bulletin of the Seismological Society of America, 103(6), 3149-3163.

Rodriguez-Marek, A., Bommer, J. J., Youngs, R. R., Crespo, M. J., Stafford, P. J., and Bahrampouri, M. (2021). Capturing epistemic uncertainty in site response. Earthquake Spectra, 37(2), 921-936.

Rodriguez-Marek, A., Montalva, G.A., Cotton, F., and Bonilla, F. (2011). Analysis of single-station standard deviation using the KiK-net data. Bulletin of the Seismological Society of America, 101, 1242-1258.

Rodriguez-Marek, A., Rathje, E.M., Bommer, J.J., Scherbaum, F., and Stafford, P.J. (2014). Application of single-station sigma and site-response characterization in a probabilistic seismic-hazard analysis for a new nuclear site. Bull. Seismol. Soc. Am. 104, 1601-1619.

Rovida A., Locati M., Camassi R., Lolli, B., Gasperini P., Antonucci A. (2022). Catalogo Parametrico dei Terremoti Italiani (CPTI15), versione 4.0. Istituto Nazionale di Geofisica e Vulcanologia (INGV). https://doi.org/10.13127/CPTI/CPTI15.4

Santulin, M., Tamaro, A., Rebez, A., Slejko, D., Sani, F., Martelli, L., Bonini, M., Corti, G., Poli, M. E., Zanferrari, A., Marchesini, A., Busetti, M., Dal Cin, M., Spallarossa, D., Barani, S., Scafidi, D., Barreca, G., and Monaco, C. (2017). Seismogenic zonation as a branch of the logic tree for the new Italian seismic hazard map - MPS16: a preliminary outline, Bollettino di Geofisica Teorica e Applicata, 58, 313-342.

Scardia, G., R. De Franco, G. Muttoni, S. Rogledi, G. Caielli, C. Carcano, D. Sciunnach, and A. Piccin (2012). Stratigraphic evidence of a Middle Pleistocene climate- driven flexural uplift in the Alps, Tectonics, 31(6).

Seed, R.B., Dickenson, S.E., Reimer, M.F., Bray, J.D., Sitar, N., Mitchell, J.K., Idriss, I.M., Kayen, R.E., Kropp, A., Harder, L.F., and Power, M.S. (1990). Preliminary report on the principal geotechnical aspects of the October 17, 1989 Loma Prieta earthquake. Report UCB/EERC-90/05, Earthquake Engineering Reasearch Center, University of California, Berkeley.

Sgobba, S., Lanzano, G., Pacor, F., Puglia, R., D'Amico, M., Felicetta, C., and Luzi, L. (2019). Spatial correlation model of systematic site and path effects for ground- motion fields in northern Italy. Bulletin of the Seismological Society of America, 109(4), 1419-1434.

Smerzini, C., Paolucci, R., and Stupazzini, M. (2011). Comparison of 3D, 2D and 1D numerical approaches to predict long period earthquake ground motion in the Gubbio plain, Central Italy. Bulletin of Earthquake Engineering, 9(6), 2007-2029.

Smerzini, C., Pitilakis, K., and Hashemi, K. (2017). Evaluation of earthquake ground motion and site effects in the Thessaloniki urban area by 3D finite-fault numerical simulations. Bulletin of earthquake engineering, 15(3), 787-812.

Stone, W.C., Yokel, F.Y., Celebi, M., Hanks, T., and Leyendecker, E.V. (1987). Engineering aspects of the September 19, 1985 Mexico earthquake. NBS Building Science Series 165, National Bureau of Standards, Washington.

Ulmer, K. J., Rodriguez- Marek, A., and Green, R. A. (2021). Accounting for epistemic uncertainty in site effects in probabilistic seismic hazard analysis. Bulletin of the Seismological Society of America, 111(4), 2005-2020.

Vanini, M., Corigliano, M., Faccioli, E., Figini, R., Luzi, L., Pacor, F., and Paolucci, R. (2018). Improving seismic hazard approaches for critical infrastructures: a pilot study in the Po Plain. Bulletin of Earthquake Engineering, 16(6), 2529-2564.

Villani, M., and Abrahamson, N.A. (2015). Repeatable site and path effects on the ground- motion sigma based on empirical data from southern California and simulated waveforms from the CyberShake platform. Bulletin of the Seismological Society of America, 105(5), 2681-2695.

Weichert, D. H. (1980), Estimation of the earthquake recurrence parameters for unequal observation periods for different magnitudes, Bull. Seismol. Soc. Am., 70, 1337–1346.

Yamanaka, H., K. Chimoto, S. Tsuno, Y. P. Dhakal, M. Amrouche, N. Yamada, S. Fukumoto, and K. Eto (2012). Estimation of S-Wave Velocity Profiles and Site Amplification Around the K-NET Tsukidate Station, Miyagi Prefecture, with Reference to Large PGA During the 2011 off Pacific Coast of Tohoku Earthquake, Japan, J. Disaster Res.7, 682-692.

Zhu, C., Pilz, M., and Cotton, F. (2020). Evaluation of a novel application of earthquake HVSR in site-specific amplification estimation. Soil Dynamics and Earthquake Engineering, 139, 106301.

Claudia Mascandola
Istituto Nazionale di Geofisica e Vulcanologia (INGV)
Via Alfonso Corti 12
20133 Milano, Italy
claudia.mascandola@ingv.it (C.M.)

Simone Barani (corresponding author)
Dipartimento di Scienze della Terra, dell'Ambiente e della Vita,
Università degli Studi di Genova,
Viale Benedetto XV 5,
16132 Genova, Italy
simone.barani@unige.it (S.B.)

Dario Albarello
Dipartimento di Scienze Fisiche, della Terra e dell'Ambiente (DSFTA),
Università degli Studi di Siena,
Strada Laterina, 8
53100 Siena, Italy
dario.albarello@unisi.it (D.A.)

List of Figure Captions

Figure 1: a) study area. The grid displayed in the map shows the computation nodes considered in the 1D ground-response analysis of Mascandola et al. (2021) and in the present PSHA. The nodes are colored according to the shape-similarity of the amplification functions in Figure 3 (to come). The active tectonic structures are from Martelli et al. (2017). b) Cross section *A-A'* from the seismo-stratigraphic model of Mascandola et al. (2021). Dark gray shows shallower sediments with $V_S < 360$ m/s; light gray indicates sediments with 360 m/s $\leq V_S <$ 800 m/s. Contour lines are every 50 m/s. The base level of the section indicates the top of the seismic bedrock defined by Mascandola et al. (2019).

Figure 2: diagram showing the computational workflow for site-specific PSHA adopted in the present study. SAPE stands for Soil Amplification Predictive Equation. Note that the rock hazard is here amended with the δ_{bas} term of the regional ground-motion attenuation model of Lanzano et al. (2016) to account for 3D basin amplification.

Figure 3: 1D and 3D amplification functions. 1D amplification functions (light and dark gray curves) are the mean amplification curves computed by Mascandola et al. (2021) for each node of the computation grid in Figure 1a (the same grayscale adopted for the grid is used here). The 3D amplification (black curve) is expressed by the δ_{bas} term of the ground-motion attenuation model of Lanzano et al. (2016).

Figure 4: (a) Bundle of soil amplification predictive models (SAPEs) relative to a period of 1 s for a grid node in the study area and (b) example SAPE for a random soil profile.

Figure 5: Uncertainty associated with the δ_{bas} term ($\sigma_{\delta_{bas}}$) and 1D amplification (σ_{1D}). The ϕ_{S2S} variability of the ground-motion attenuation model of Lanzano et al. (2016) ($\phi_{S2S-NI15}$) and the one computed here for the Po Plain sites only ($\phi_{S2S-PoPlain}$) are also shown.

Figure 6: logic tree. MA1: source zone model (Santulin et al., 2017); G & R: Gutenberg and Richter model; M_{max}: maximum magnitude; ITA18: GMPE of Lanzano et al. (2019); σ_μ: standard deviation of the mean (logarithmic) ground motion; ϕ_{SS}: event-corrected single-station standard deviation;

$\sigma_{\phi_{SS}}$: standard deviation of ϕ_{SS}; δ_{bas}: amplification term relative to 3D basin effects; $\sigma_{\delta_{bas}}$: standard deviation of δ_{bas}.

Figure 7: mean site-specific, partially non-ergodic hazard maps corresponding to a return period of 475 years: a) PGA; b) $Sa(1\ s)$; c) $Sa(1.6\ s)$; d) $Sa(3\ s)$. Contour lines indicate the resonance periods of the soft sediments above seismic bedrock (modified from Mascandola et al. (2019)). The tectonic structures shown in Figure 1a are superimposed.

Figure 8: $V_{S,30}$-driven ergodic hazard maps corresponding to a return period of 475 years: a) PGA; b) $Sa(1\ s)$; c) $Sa(1.6\ s)$; d) $Sa(3\ s)$. The tectonic structures shown in Figure 1a are superimposed.

Figure 9: percentage differences between the site-specific, partially non-ergodic hazard values in Figure 7 and those in Figure 8 obtained through the application of the conventional $V_{S,30}$-driven ergodic approach. The dashed line marks the study area.

Figure 10: epistemic uncertainty (difference between the ground-motion values for a return period of 475 years corresponding to the 84th and 16th percentiles, $\Delta_{84\text{-}16}$) in the site-specific hazard results. The dashed line marks the study area.

Figure 11: a) event-corrected standard deviation (ϕ_{SS}) as a function of moment magnitude (M_w); b) standard deviation of the mean (logarithmic) ground motion (σ_μ) as a function of spectral period T.

Figure 12: boxplots showing a) the sensitivity of the mean hazard to the 3D amplification, and b) the percentage contribution of the uncertainties affecting the 1D (dark gray) and 3D (light gray) amplification (in terms of $\Delta_{84\text{-}16}$) to the total epistemic uncertainty in the hazard. Statistics are computed considering the entire study area (i.e., all computation nodes in Figure 1a). The line in the middle of each box indicates the median. The box edges correspond to the 25th and 75th percentiles. The whiskers are the minimum and maximum values that do not exceed 1.5 times the interquartile range.

Figure 13: Uniform Hazard Spectra (UHS) corresponding to a mean return period of 475 years for four main cities in the Po Plain area. The dashed area roughly indicates the range of periods where the hazard results are affected by the lower resolution of the 1D site-response model.

Figure 1

Click here to access/download;Figure;Fig1.jpg

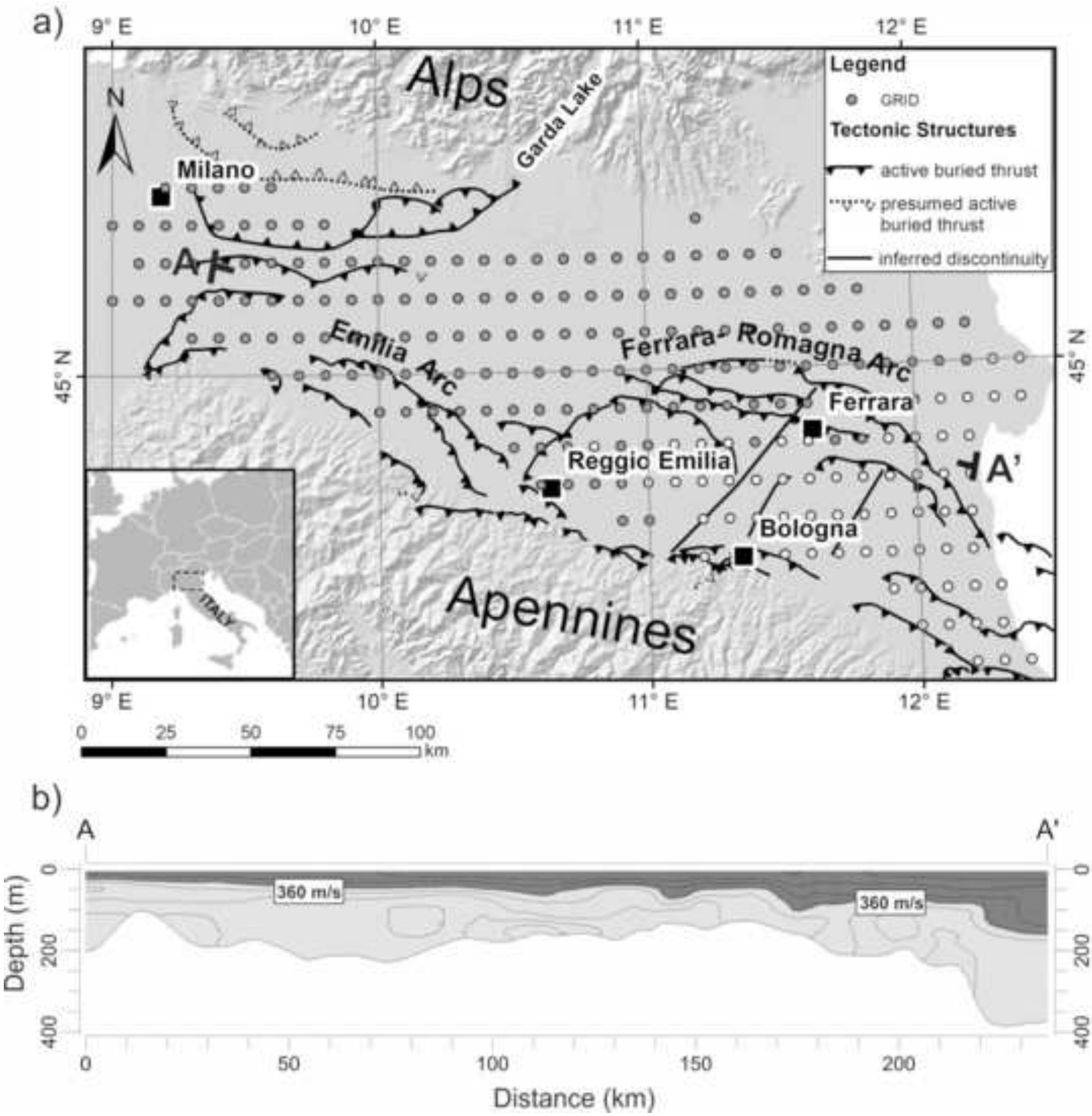

Figure 2

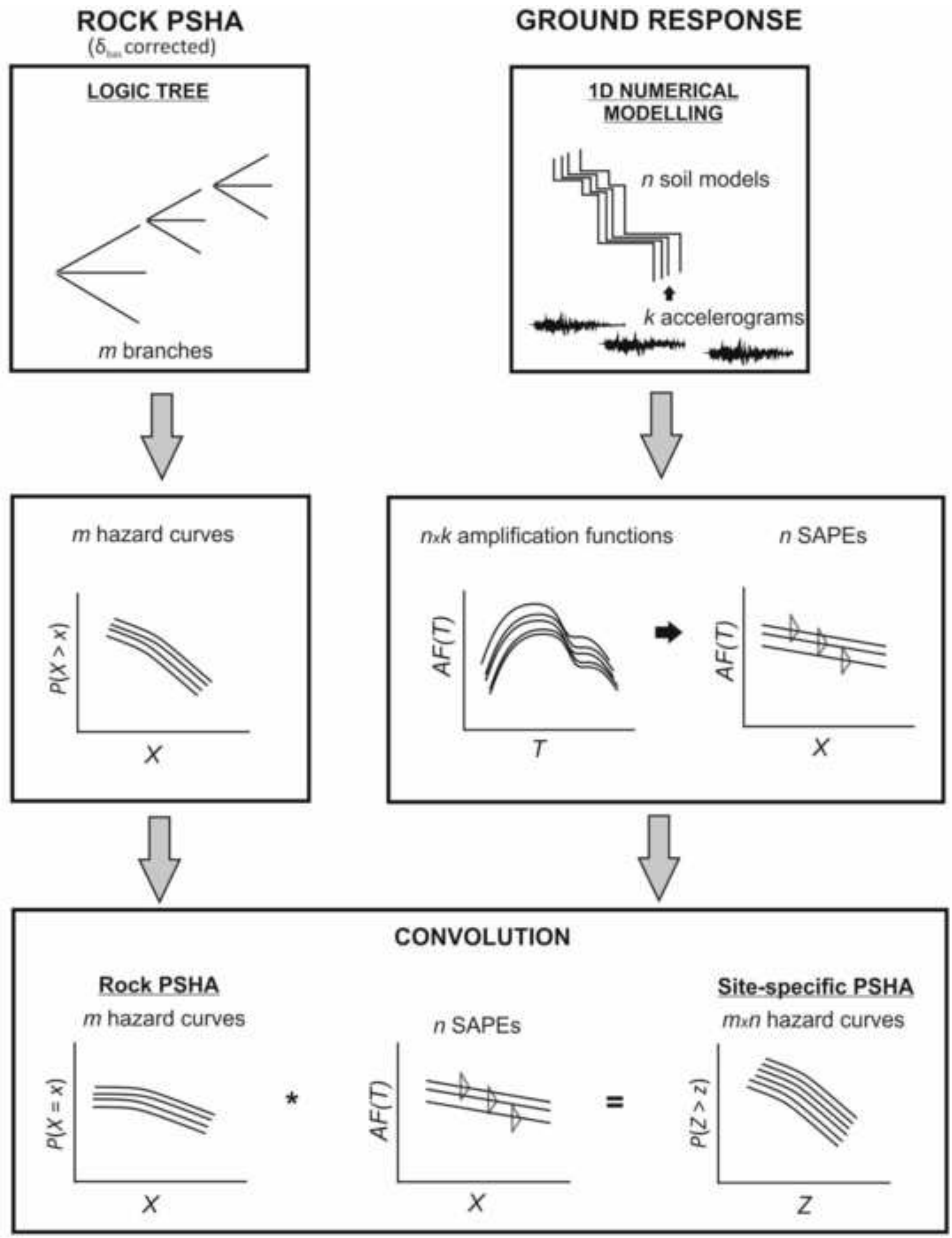

ROCK PSHA
(δ corrected)
LOGIC TREE
m branches
GROUND RESPONSE
1D NUMERICAL MODELLING
n soil models
k accelerograms
m hazard curves
P(X > x)
X
nxk amplification functions
n SAPEs
AF(T)
T
AF(T)
X
CONVOLUTION
Rock PSHA
m hazard curves
P(X = x)
X
*
n SAPEs
AF(T)
X
=
Site-specific PSHA
mxn hazard curves
P(Z > z)
Z

Figure 3

Click here to access/download;Figure;Fig3.jpg

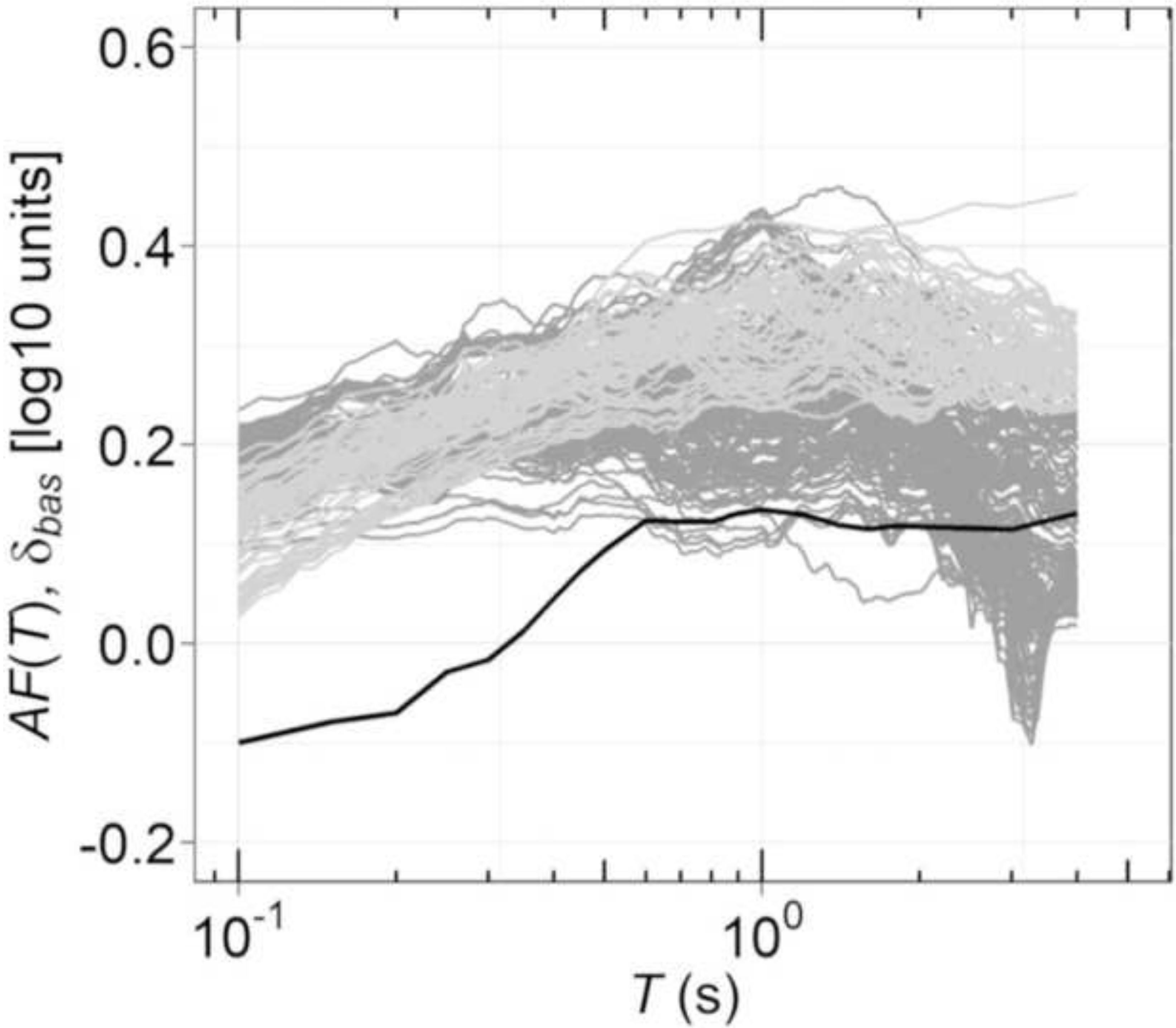

Figure 4

Click here to access/download;Figure;Fig4.jpg

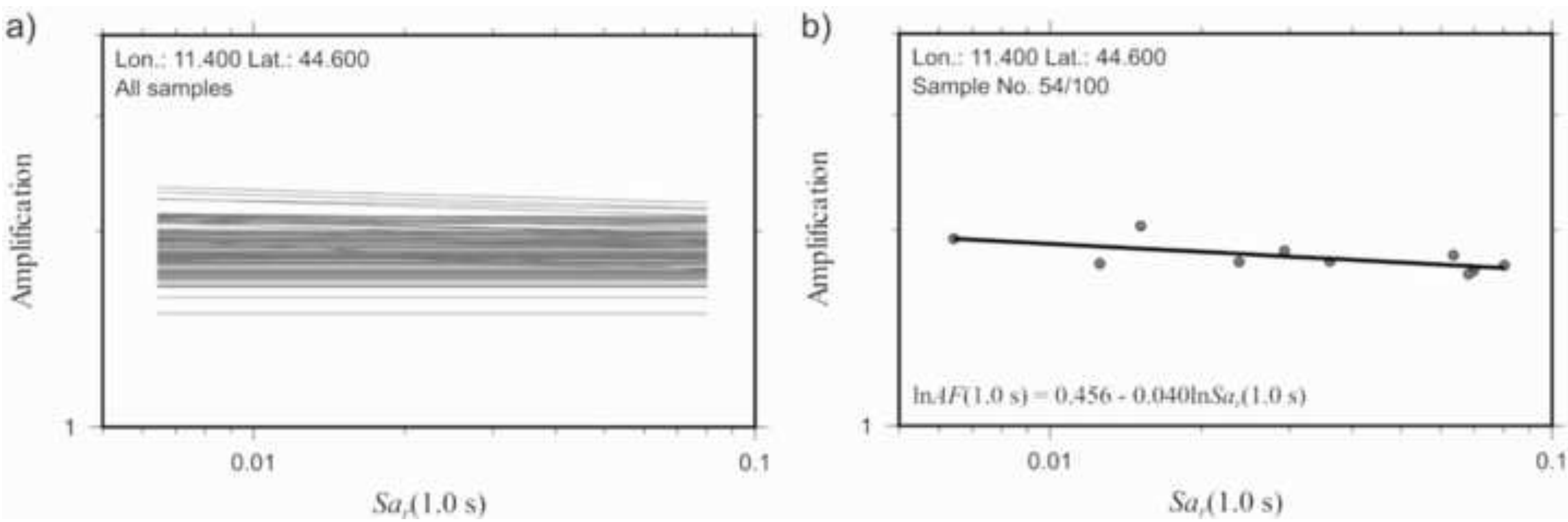

Figure 5

Click here to access/download;Figure;Fig5.jpg

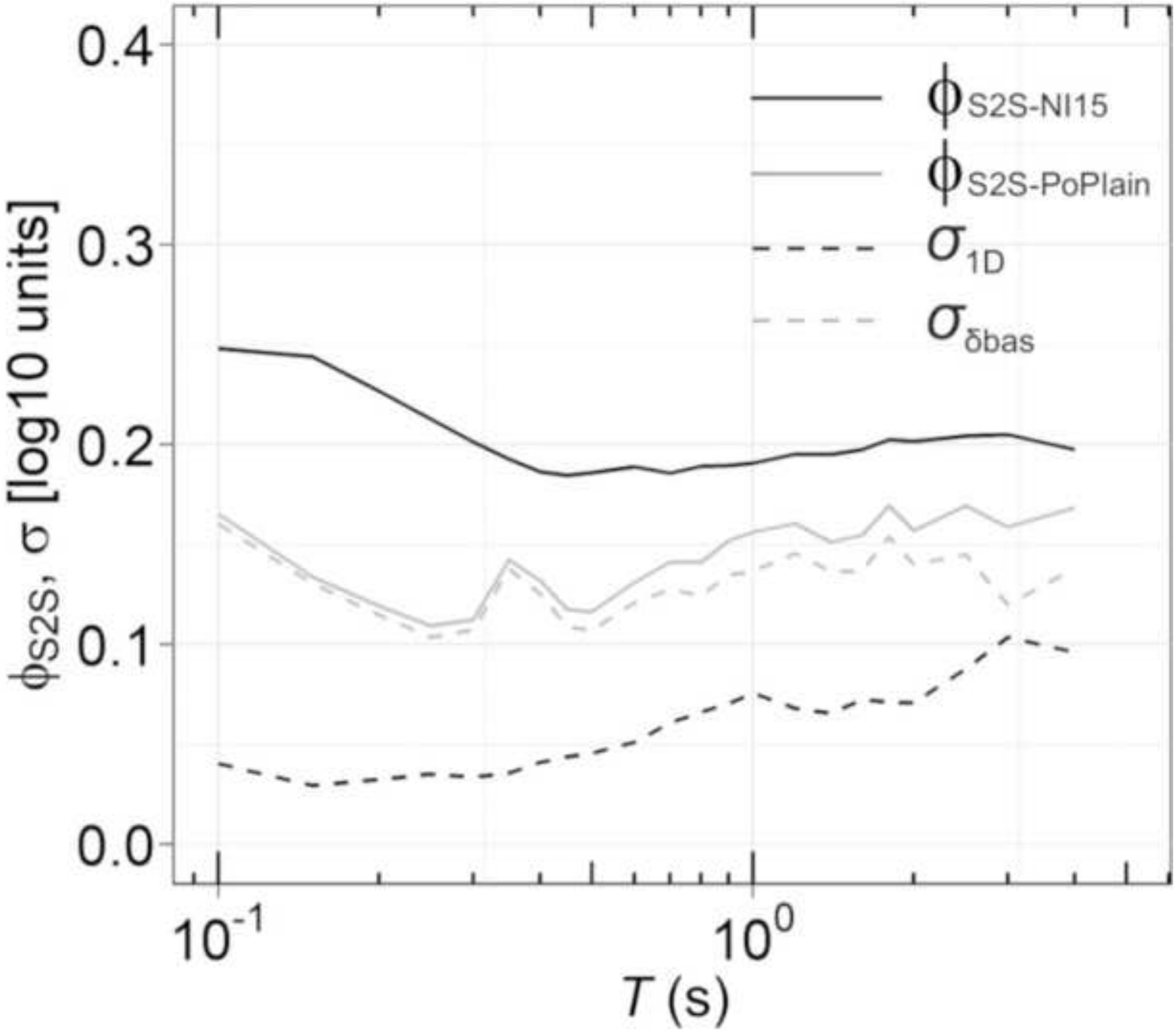

Figure 6

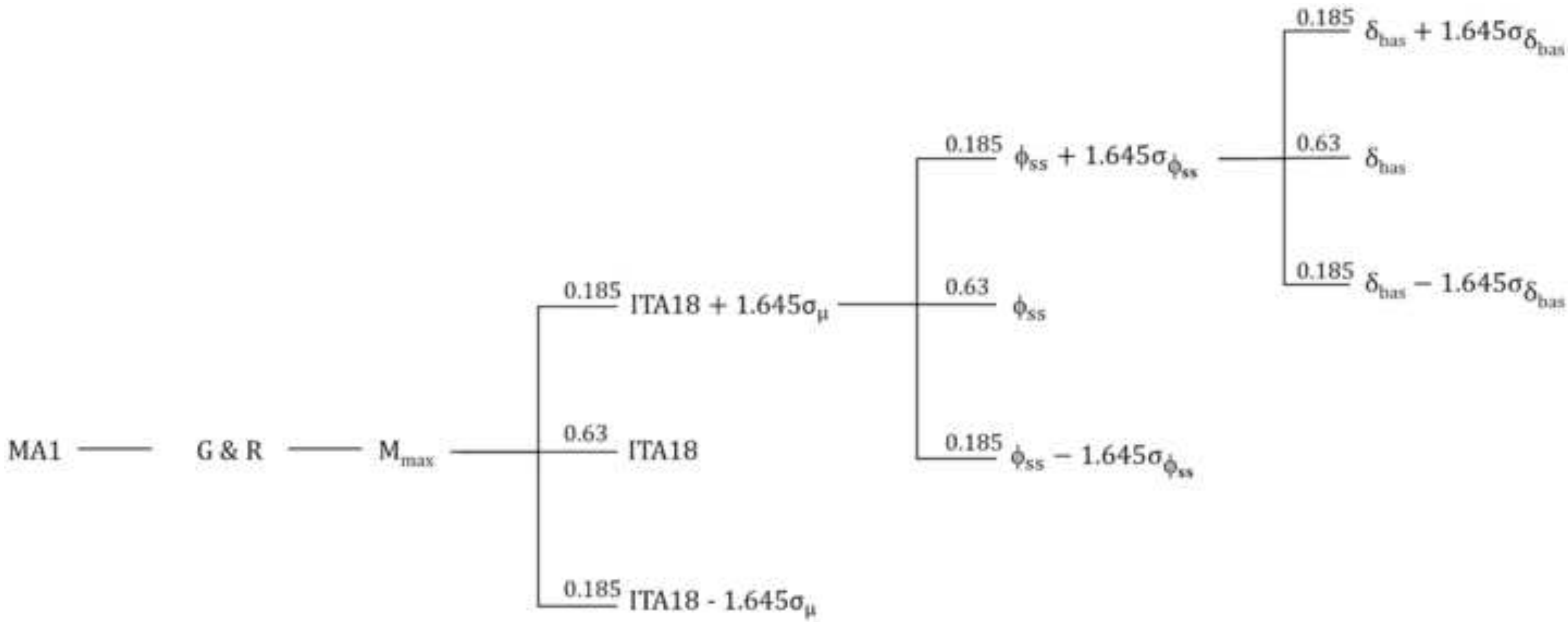

MA1
G & R
M_{max}
0.185
ITA18 + $1.645\sigma_{\mu}$
0.63
ITA18
0.185
ITA18 - $1.645\sigma_{\mu}$
0.185
$\phi_{ss} + 1.645\sigma_{\phi_{ss}}$
0.63
ϕ_{ss}
0.185
$\phi_{ss} - 1.645\sigma_{\phi_{ss}}$
0.185
$\delta_{bas} + 1.645\sigma_{\delta_{bas}}$
0.63
δ_{bas}
0.185
$\delta_{bas} - 1.645\sigma_{\delta_{bas}}$

Figure 7

Click here to access/download;Figure;Fig7.jpg

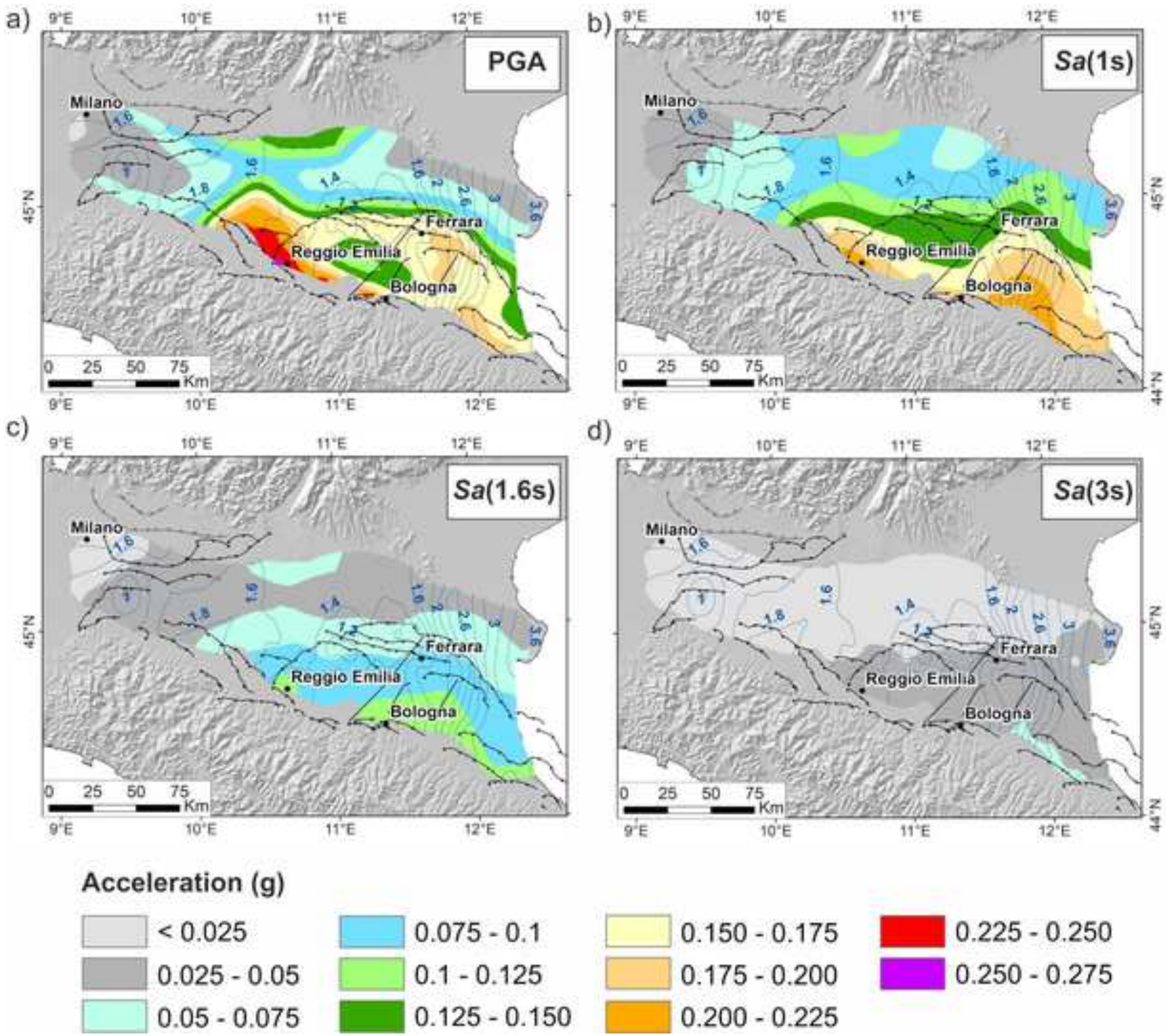

Figure 8

Click here to access/download;Figure;Fig8.jpg

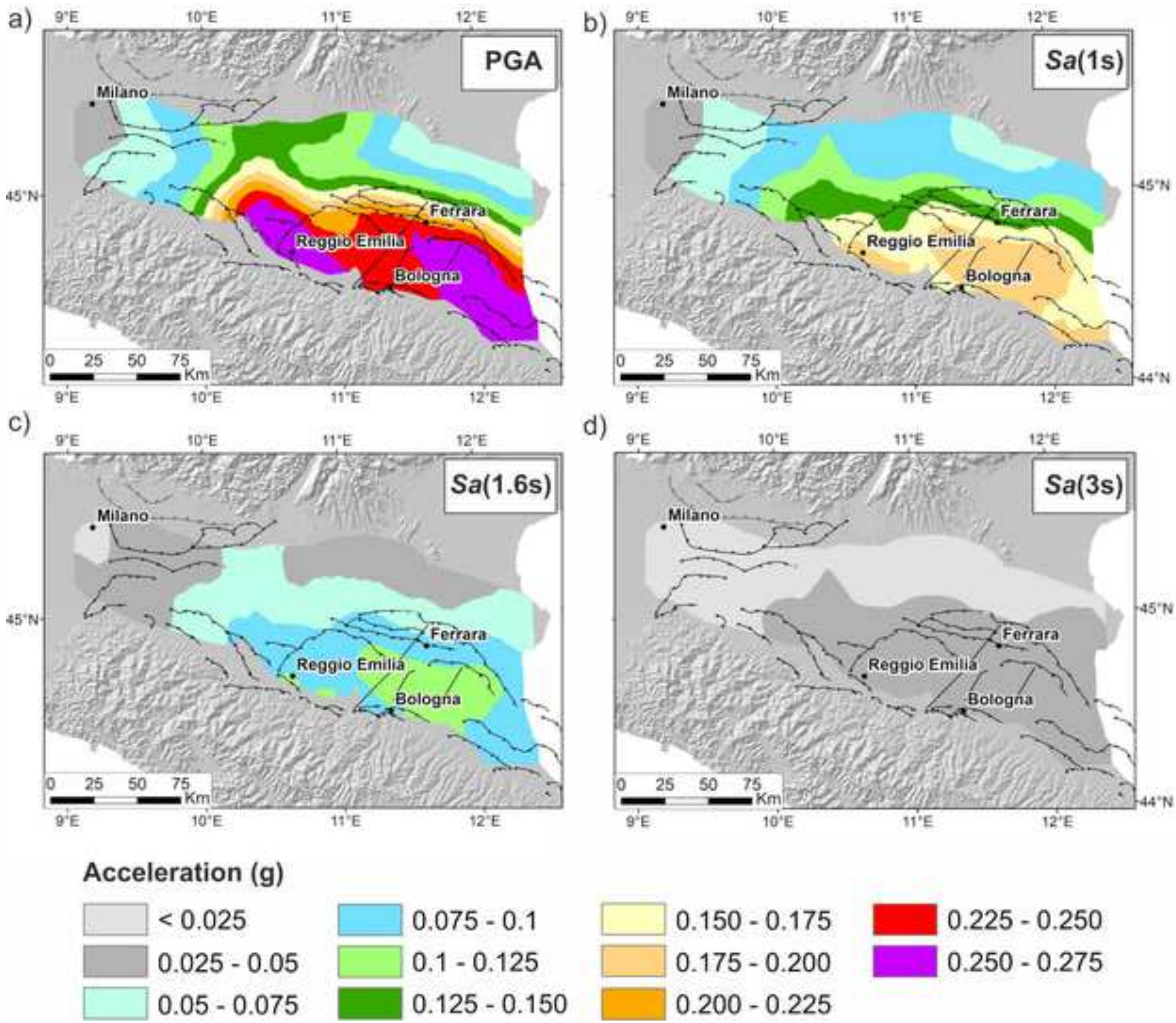

Figure 9

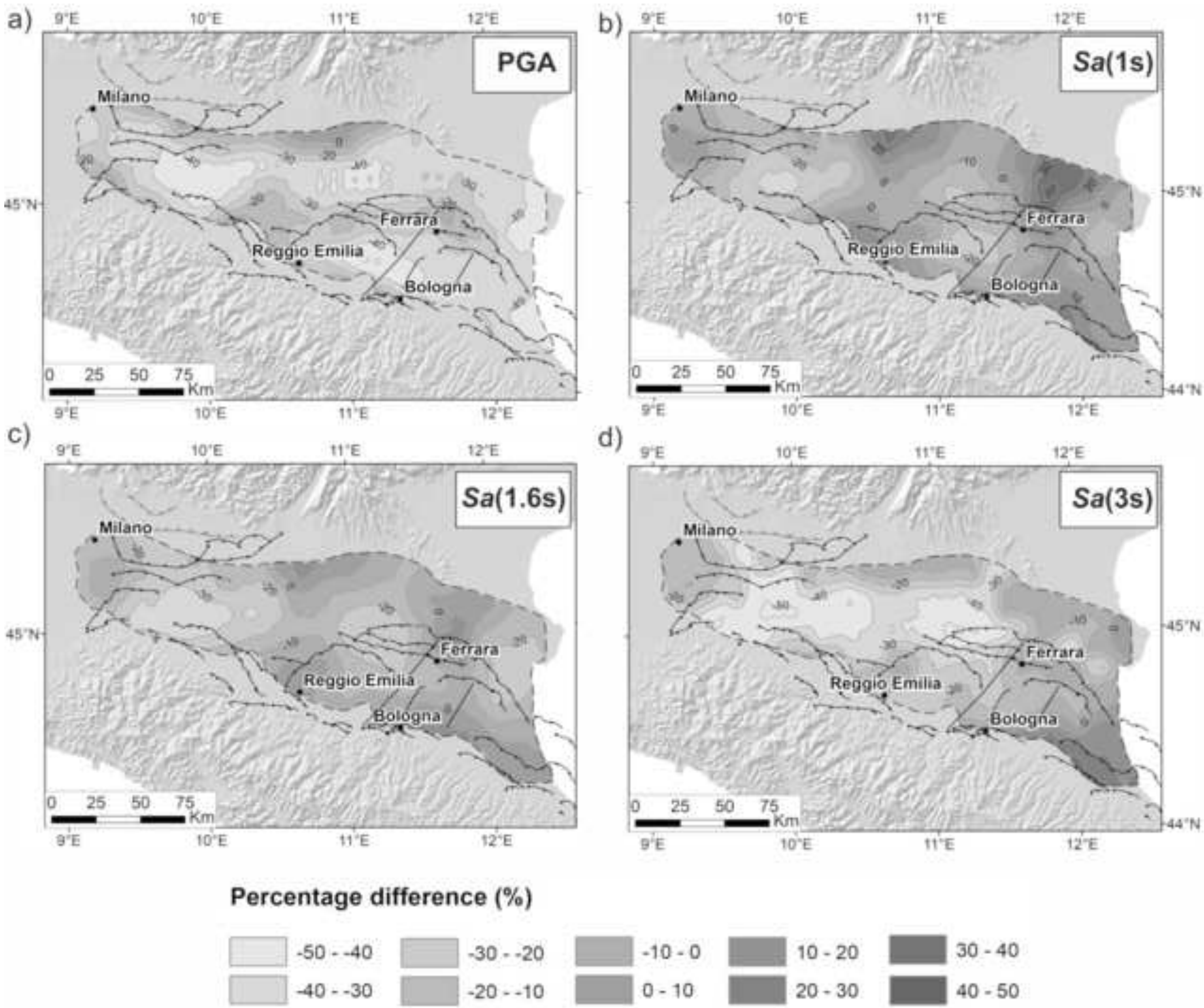
a)
PGA
b)
Sa(1s)
c)
Sa(1.6s)
d)
Sa(3s)
Milano
Ferrara
Reggio Emilia
Bologna
9°E
10°E
11°E
12°E
45°N
44°N
0 25 50 75 Km
Percentage difference (%)
-50 - -40
-40 - -30
-30 - -20
-20 - -10
-10 - 0
0 - 10
10 - 20
20 - 30
30 - 40
40 - 50

Figure 10

Click here to access/download;Figure;Fig10.jpg

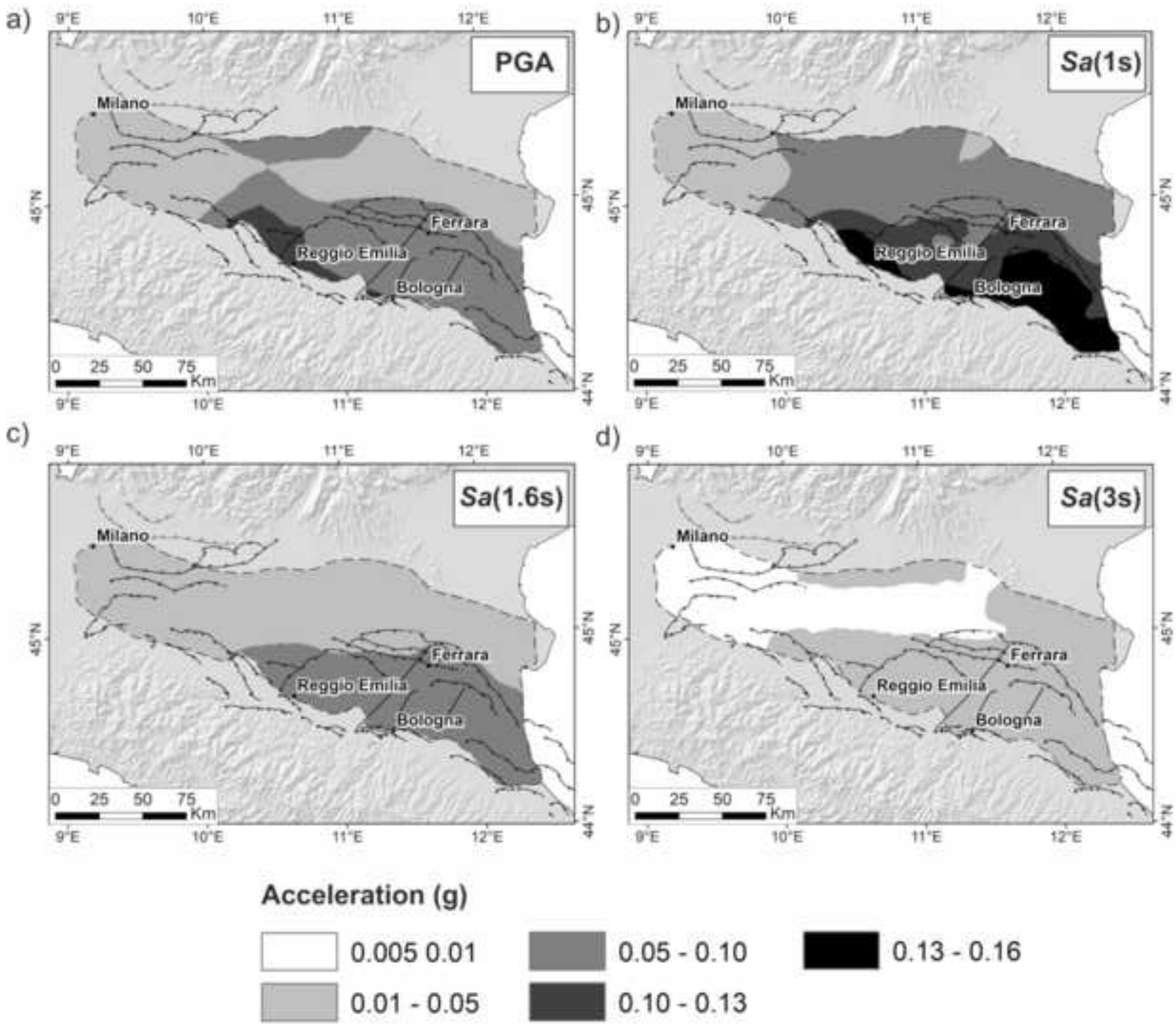

Figure 11

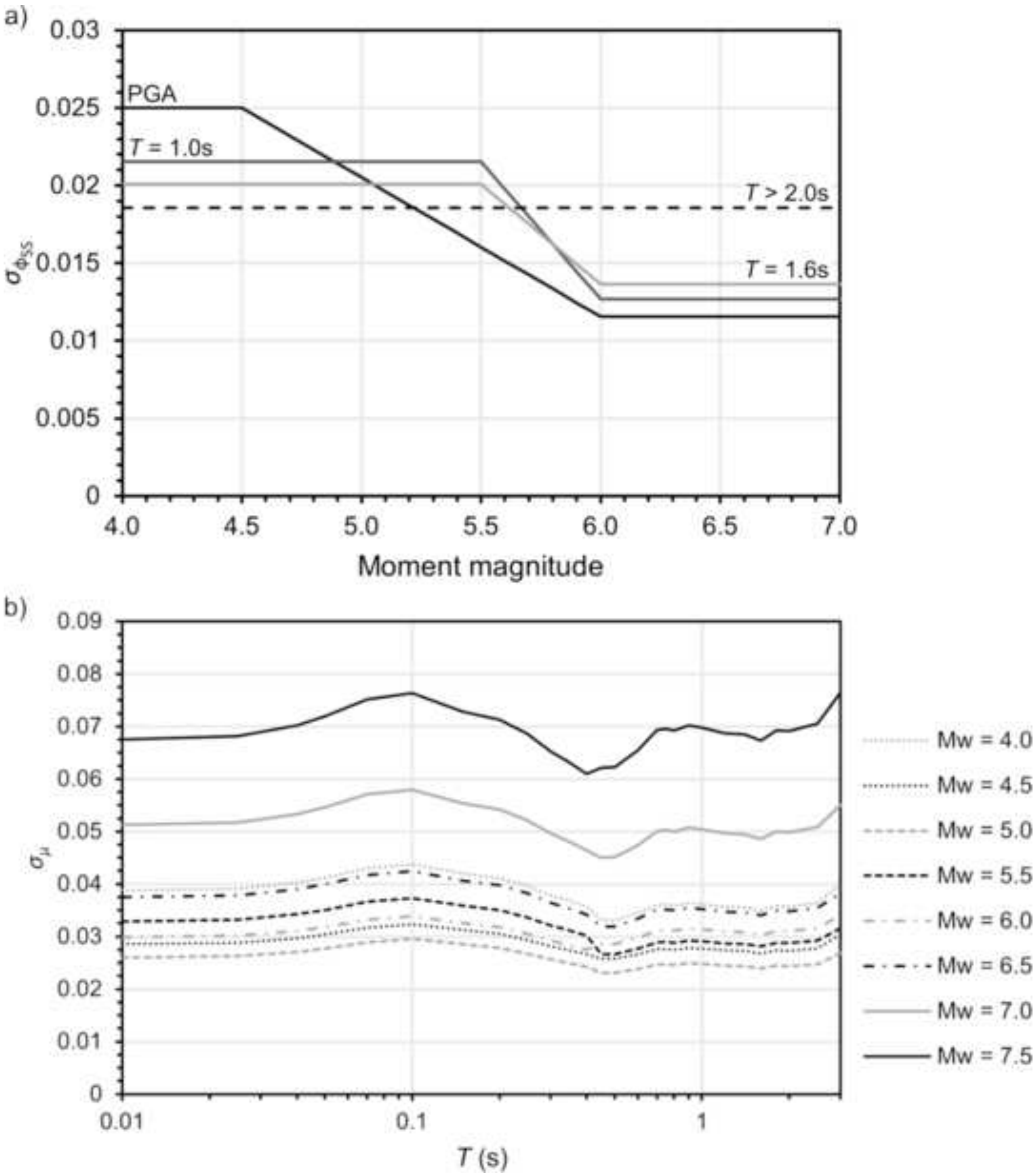

a)
PGA
T = 1.0s
T > 2.0s
T = 1.6s
σφSS
0.03
0.025
0.02
0.015
0.01
0.005
0
4.0
4.5
5.0
5.5
6.0
6.5
7.0
Moment magnitude
b)
σμ
0.09
0.08
0.07
0.06
0.05
0.04
0.03
0.02
0.01
0
0.01
0.1
1
T (s)
Mw = 4.0
Mw = 4.5
Mw = 5.0
Mw = 5.5
Mw = 6.0
Mw = 6.5
Mw = 7.0
Mw = 7.5

Figure 12 Click here to access/download;Figure;Fig12.jpg

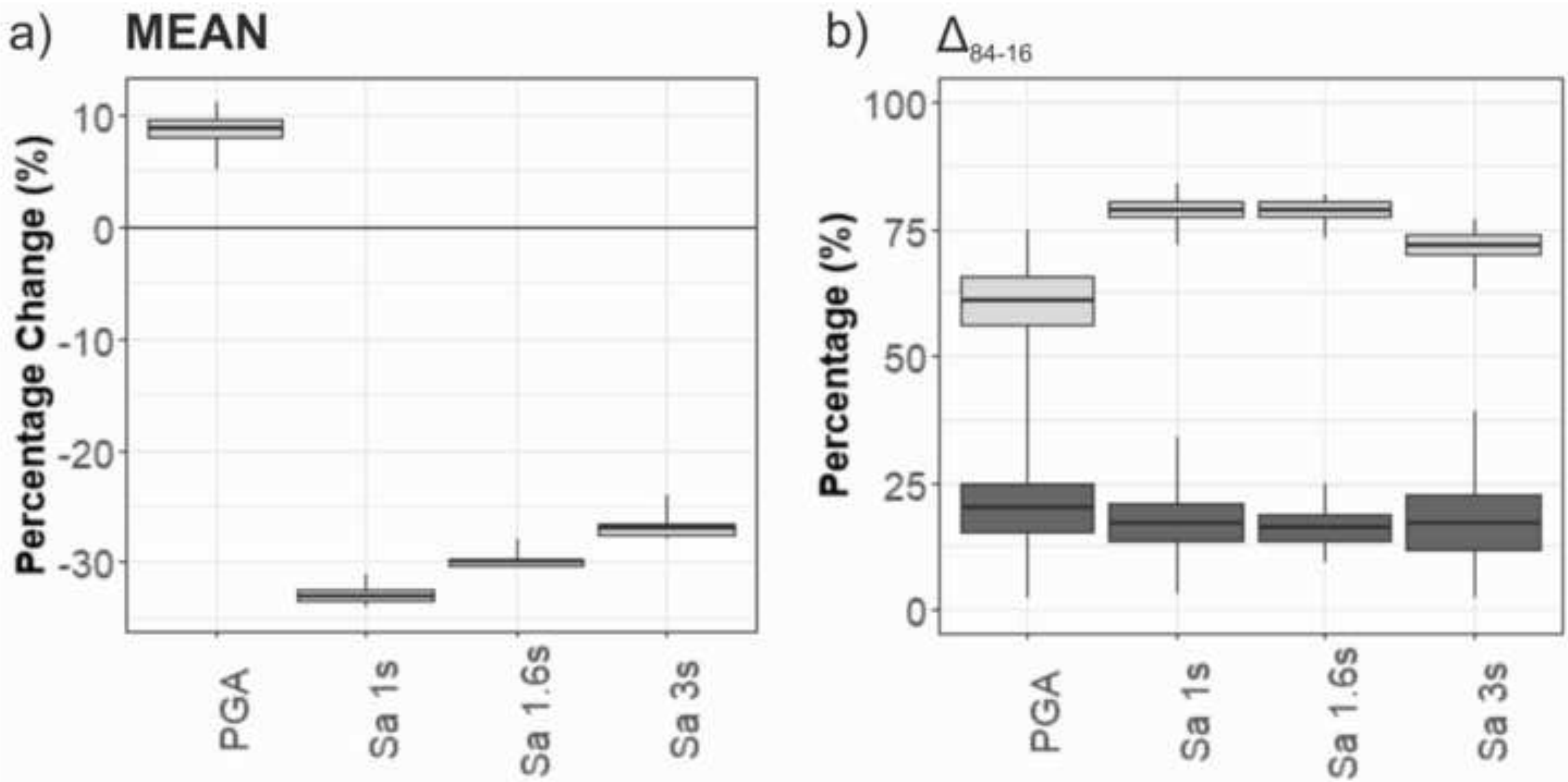

Figure 13 Click here to access/download;Figure;Fig13.jpg

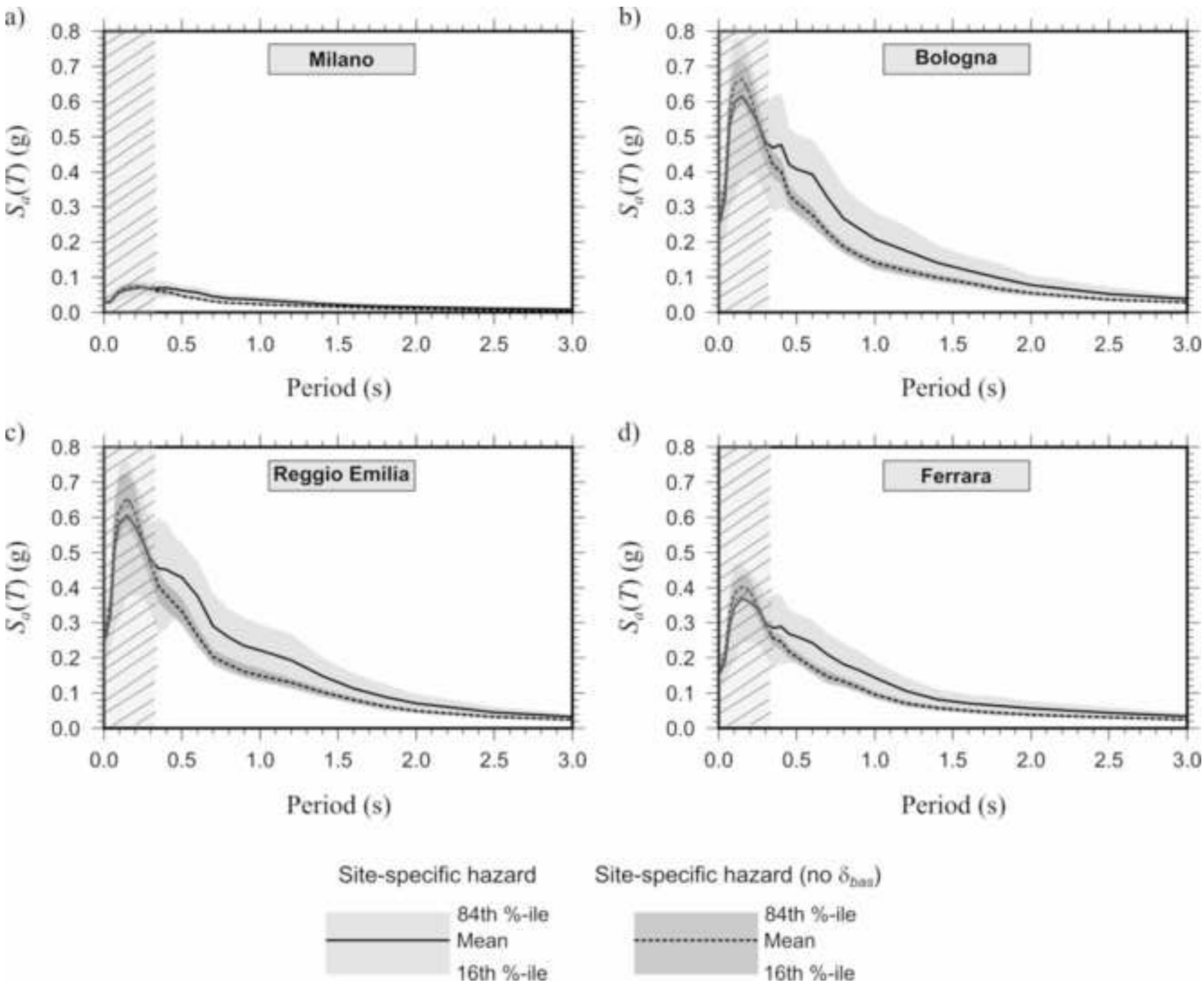

Electronic Supplement to

Impact of Site-Response Characterization on Probabilistic Seismic Hazard in the Po Plain (Italy)

by Claudia Mascandola, Simone Barani and Dario Albarello

The present electronic supplement includes:

- Appendix S1, which describes the basic input data used in the hazard assessment; especially, it describes the seismogenic model used in the computations along with its parameterization.
- Appendix S2, which presents ergodic hazard maps for rock conditions.

Appendix S1

For the purpose of hazard computations, we used the source zone model of Santulin et al (2017). For each zone, we adopted the truncated Gutenberg and Richter model (Cornell and Vanmarcke, 1969) to define the magnitude-frequency distribution. We computed the values of its parameters (i.e., intercept, *a*, and slope, *b*, coefficients) from the CPTI15 catalog (Rovida et al., 2022; see Data and Resources) deprived of dependent events according to the assumption that earthquakes occur following a Poisson process. To this end, we used the maximum likelihood approach of Weichert (1980). Moreover, M_{min} is set to 4.0 for all zones, and M_{max} is assumed equal to the value of M_{max1} in Santulin et al (2017), which is defined as the highest magnitude value between the maximum magnitude derived from the CPTI15 catalog and the maximum magnitude reported in the Database of Individual Seismogenic Sources (DISS Working Group, 2015; see Data and Resources) in specific macro-areas (see Figure 8 in Santulin et al., 2017), increased by the associated standard deviation. For the source zones that are deemed to affect the hazard in the study area, the values of such parameters are reported in Table S1, along with those of the prevalent rake angle and seismogenic depth (again from Santulin et al. (2017)). The map of the source zones is shown in Figure S1.

Table S1: parameterization of the source zones used in the hazard computations. *a* and *b* are the coefficients of the Gutenberg and Richter relation, M_{max} is the maximum magnitude, and *hd* indicates the seismogenic depth. The rake angle is used to assign a prevalent style of faulting to each source.

Zone ID	*a*	*b*	M_{max}	rake (°)	*hd* (km)
101	3.166	0.978	6.9	90	8
102	3.177	1.000	6.9	180	12
103	3.231	1.027	6.9	90	10
106	4.016	1.181	6.9	180	15
107	4.603	1.295	6.9	180	15
108	2.194	0.823	6.9	170	10
110	4.777	1.285	6.9	180	15
112	2.843	0.953	6.9	90	9
113	2.336	0.857	6.9	90	8
114	3.633	1.054	6.9	180	12
301	2.651	0.947	6.6	90	5
303	2.737	0.950	6.6	0	6
304	2.377	0.846	6.7	ND	5
305	3.953	1.309	6.5	90	34
306	4.346	1.214	6.7	ND	11
307	3.229	1.025	6.7	-90	5
310	2.217	0.818	6.7	-90	5

311	2.107	0.812	6.7	0	6
511	4.087	1.201	6.5	0	8
513	3.363	1.006	7.1	0	18
515	3.685	1.048	7.4	-90	5
516	2.207	0.789	7.1	-90	8
517	5.091	1.380	7.1	90	20
519	3.416	1.015	7.1	90	10
521	3.486	1.100	7.4	0	9
529	2.810	0.941	7.1	0	6
530	4.458	1.264	7.1	90	6
531	2.581	0.838	7.1	-90	6
532	3.910	1.133	7.4	-90	6
535	3.162	1.002	7.4	0	6
536	3.985	1.202	7.1	0	6
537	1.844	0.645	7.1	90	6
539	3.541	0.930	7.4	-90	6
540	2.734	0.951	7.4	-90	6
541	3.054	0.936	6.5	-90	6
833	3.354	1.100	6.5	-90	6
933	2.670	0.906	7.4	-90	6
938	3.035	0.965	7.1	90	6

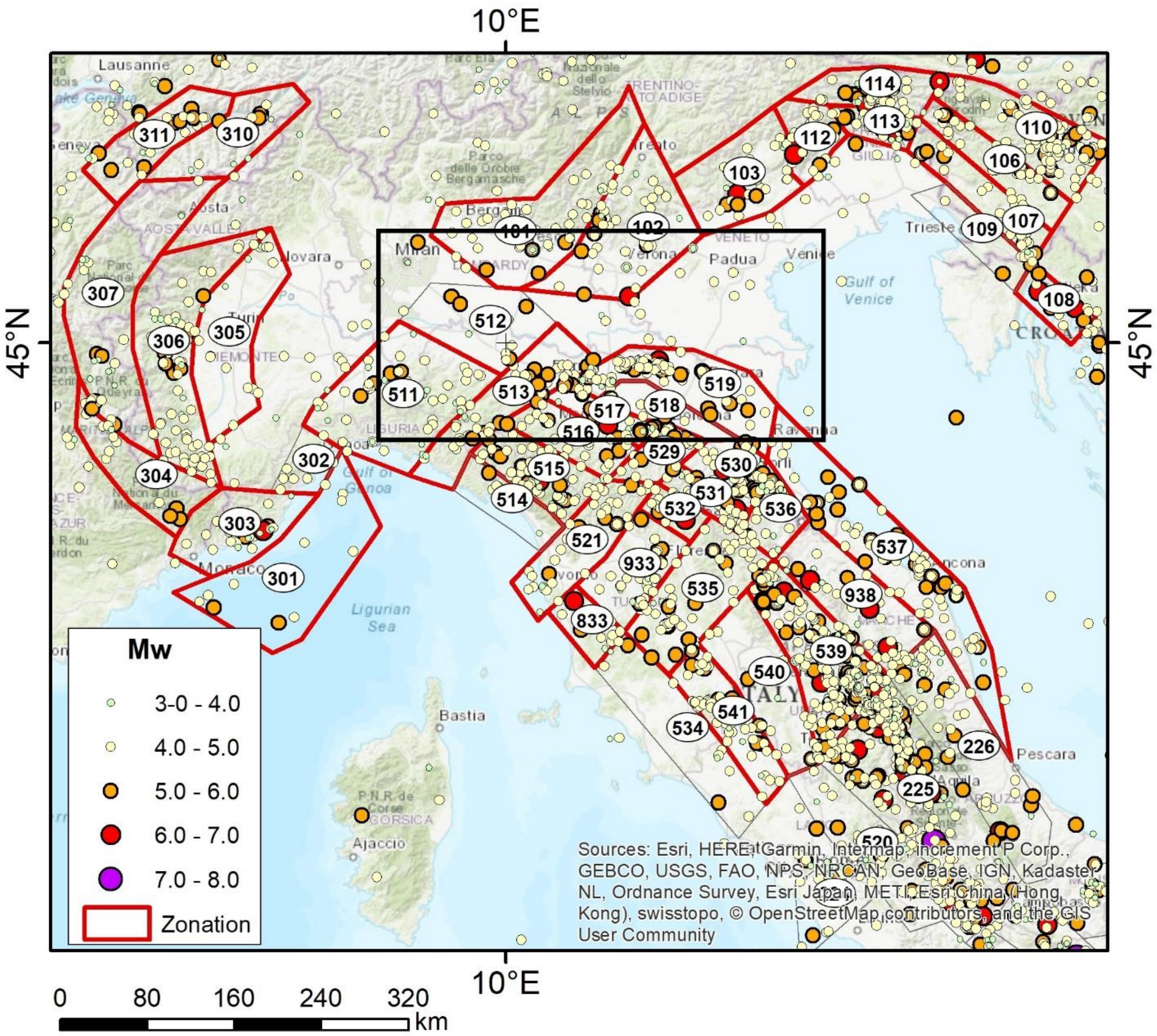

Figure S1: map of the seismogenic zonation of Santulin et al. (2017). The source zones considered in the present study are in red (see also Table S1). Zones #109, #302, #512, #514, #518, and #534 are not considered in the hazard assessment because of their very low seismicity (i.e., too small a number of earthquakes), which does not allow for reliable estimates of the *a* and *b* coefficients of the Gutenberg and Richter relation. The black box indicates the study area. Earthquake epicenters are from the CPTI15 catalog (Rovida et al., 2022).

Appendix S2

Figure S2 shows the ergodic hazard maps for rock conditions associated with a return period of 475 years for the same spectral periods considered in the main body of the manuscript.

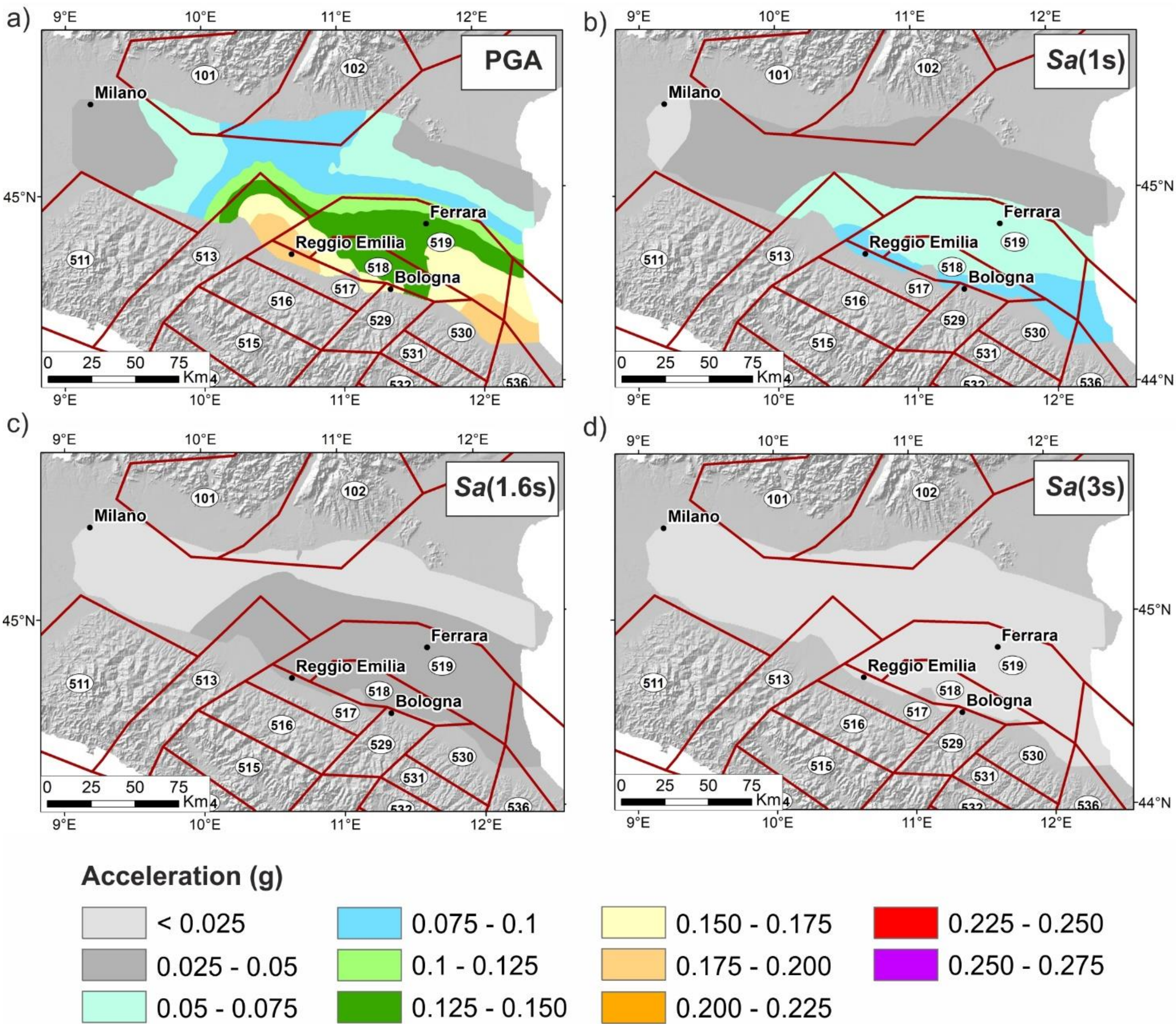

Figure S2: ergodic hazard maps for rock conditions ($V_{S,30} \geq 800\ \mathrm{m/s}$) associated with a return period of 475 years for: a) PGA; b) $Sa(1\ \mathrm{s})$; c) $Sa(1.6\ \mathrm{s})$; d) $Sa(3\ \mathrm{s})$. The seismogenic zones adopted in the hazard analysis (Santulin et al. 2017) are superimposed.